Deep-Water Formation and Meridional Overturning in a High-Resolution Model of the North Atlantic

CLAUS W. BÖNING

Institut für Meereskunde an der Universität Kiel, Kiel, Germany

FRANK O. BRYAN AND WILLIAM R. HOLLAND

National Center for Atmospheric Research, Boulder, Colorado

RALF DÖSCHER

Alfred-Wegener-Institute for Polar and Marine Research, Bremerhaven, Germany

(Manuscript received 13 May 1994, in final form 9 August 1995)

ABSTRACT

The authors use different versions of the model of the wind- and thermohaline-driven circulation in the North and Equatorial Atlantic developed under the WOCE Community Modeling Effort to investigate the mean flow pattern and deep-water formation in the subpolar region, and the corresponding structure of the basin-scale meridional overturning circulation transport. A suite of model experiments has been carried out in recent years, differing in horizontal resolution (1° × 1.2°, 1/3° × 0.4°, 1/6° × 0.2°), thermohaline boundary conditions, and parameterization of small-scale mixing. The mass transport in the subpolar gyre and the production of North Atlantic Deep Water (NADW) appears to be essentially controlled by the outflow of dense water from the Greenland and Norwegian Seas, in the present model simulated by restoring conditions in a buffer zone adjacent to the boundary near the Greenland–Scotland Ridge. Deep winter convection homogenizes the water column in the center of the Labrador Sea to about 2000 m. The water mass properties (potential temperature about 3°C, salinity about 34.9 psu) and the volume (1.1×10^5 km^3) of the homogenized water are in fair agreement with observations. The convective mixing has only little effect on the net sinking of upper-layer water in the subpolar gyre. Sensitivity experiments show that the export of NADW from the subpolar North Atlantic is more strongly affected by changes in the overflow conditions than by changes in the surface buoyancy fluxes over the Labrador and Irminger Seas, even if these suppress the deep convection completely. The host of sensitivity experiments demonstrates that realistic meridional overturning and heat transport distributions for the North Atlantic (with a maximum of 1 PW) can be obtained with NADW production rates of 15–16 Sv, provided the spurious upwelling of deep water that characterizes many model solutions in the Gulf Stream regime is avoided by adequate horizontal resolution and mixing parameterization.

1. Introduction

An important component of the present state of earth's climate is the northward, cross-equatorial transport of heat in the Atlantic Ocean, associated with the release of a large amount of heat to the atmosphere and transformation of warm, upper-layer water to cold North Atlantic Deep Water (NADW) in subarctic regions. Paleoclimatic records (Broecker 1991) and coupled ocean–atmosphere models (Delworth et al. 1993) suggest that the ocean's thermohaline circulation may play a crucial role in climate variations. Ocean models of different complexity indicate that feedbacks between the oceanic transports and the atmosphere lead to the existence of multiple equilibrium states and the possibility of rapid transitions and oscillations on different timescales (e.g., Weaver et al. 1993; Weisse et al. 1994). At present, however, the actual mechanisms that govern the thermohaline circulation are only poorly known. An identification and quantitative assessment of the main processes that determine the formation and transport of deep water in the North Atlantic and their accurate representation in numerical models are of considerable interest and a prerequisite for an understanding of natural climate variations and anthropogenic changes.

In the present study we shall use the suite of models of the wind- and thermohaline-driven circulation developed under the World Ocean Circulation Experiment (WOCE) Community Modeling Effort (CME) to

Corresponding author address: Dr. Claus W. Böning, Institut für Meereskunde an der Universität Kiel, Düsternbrooker Weg 20, D-24105 Kiel, Germany.

(i) establish the ability of a high-resolution model in realistic geometry, for prescribed monthly atmospheric forcing functions and boundary conditions, to simulate the observed features of the three-dimensional circulation in the subpolar North Atlantic

(ii) examine the sensitivity to horizontal resolution and the role of different processes, that is, wind and thermohaline forcing, for the structure and transport of the subpolar gyre

(iii) address the questions of which areas and mechanisms in the subpolar North Atlantic contribute to the renewal of deep water, and which factors control the net deep-water formation rate.

In addition, the paper provides a synthesis of results from many model cases to illuminate the main processes and model factors that govern the structure and strength of the meridional overturning circulation and associated poleward transport of heat in the North Atlantic.

Various source regions and different processes have been identified to contribute to the formation of NADW in the subarctic Atlantic. The heaviest components originate from arctic intermediate waters formed by middepth winter convection in regions north of Iceland, spilled out through Denmark Strait, across the Iceland–Faeroe Ridge and through Faeroe Bank Channel (Smethie and Swift 1989). The total overflow rate of 5–6 Sv (Sv $\equiv 10^6$ m^3 s^{-1}) (a compilation of recent estimates is given by Dickson et al. 1991) is believed to be enhanced along the descent of the outflowing waters south of the ridges by entrainment of overlying, less dense water, roughly doubling the initial volume transports (Price and Baringer 1994). Much less clear is the role of the Labrador Sea where, in six out of ten winters, deep convection leads to a homogenization to depths of about 2000 m (Lazier 1988). While the imprint of Labrador Sea Water (LSW) can be detected in the hydrographic properties and tracer signatures of upper NADW in lower latitudes (Fine and Molinari 1988), the dynamical effect of that water mass transformation on the net southward transport of NADW is largely unknown.

Numerical models of the thermohaline circulation were often characterized by a too weak overturning rate and heat transport in the subtropical North Atlantic. In a comprehensive study of the mean and seasonal heat budgets of the Atlantic Ocean using a 2° × 2° model with realistic bathymetry and climatological, monthly mean forcing, Sarmiento (1986) obtained a maximum meridional overturning of 12.8 Sv and annual mean poleward heat transport of 0.86 PW at 24.5°N. Several model studies in recent years showed that the overturning critically depends on a number of model factors like the specification of the (poorly known) heat and freshwater fluxes over the subarctic Atlantic (Maier-Reimer et al. 1993; England 1993; Gerdes and Köberle 1995). However, sensitivity studies of the global or basin-scale thermohaline circulation were typically based on models with a horizontal resolution of only 2° to 5° that do not capture the actual, energetic elements of ocean circulation such as boundary currents and fronts. A question of considerable interest, therefore, is how robust the patterns and sensitivities of deep-water formation, meridional overturning, and heat transport are against refinements in horizontal resolution.

At present, studies of the sensitivity of ocean circulation in thermodynamic equilibrium with eddy-resolving models are computationally impractical. There are some important aspects of the thermohaline circulation in the North Atlantic, however, that may be addressed with high-resolution models, and integration times of a few decades. The spinup of the circulation can be thought of as essentially a two-step process: a fast dynamic response to the thermohaline fluxes in the high latitudes, involving continental shelf waves, equatorial Kelvin waves, and midlatitude Rossby waves (Kawase 1987) that leads to a "quasi-dynamic" equilibrium of meridional overturning and heat transport in the North Atlantic within 10–15 years (Döscher et al. 1994; Gerdes and Köberle 1995); and a very slow adjustment to thermodynamic equilibrium governed by the weak diapycnic fluxes and advection in the deep ocean interior (Bryan 1987). Here we are primarily interested in the dynamical, decadal-scale aspect of the thermohaline circulation and its response to atmospheric forcing, and not the secular aspects associated with the evolution of water mass properties in the deep ocean interior.

Numerous model experiments based on the original CME (Bryan and Holland 1989) have been carried out in recent years differing in horizontal resolution, mixing parameterization, wind stress, and thermohaline forcing. The basic CME cases, which used monthly mean climatological data for the forcing fields at the surface and for the boundary conditions at the south (15°S) and north (65°N) ends of the domain, showed the typical deficits in the mean overturning circulation and northward heat transport that are characteristic for a variety of North Atlantic models: a southward transport of NADW at 25°N being too low by 7–10 Sv, in particular because of a lack of southward transport in the depth and temperature range of lower NADW; a northward heat transport with a maximum of 0.6–0.7 PW, significantly below the 1.2 ± 0.3 PW inferred from transoceanic sections at that latitude (Hall and Bryden 1982, hereafter HB; Roemmich and Wunsch 1985, hereafter RW). Specific aspects of these shortcomings have been addressed in different studies: Holland and Bryan (1994) examine the mean zonally integrated transports of mass and heat for a sequence of experiments with a non-eddy-resolving version of the CME and different wind and freshwater flux conditions at the surface, and find a strong sensitivity to the formulation of the open boundary conditions at the north

and south ends of the domain. Döscher et al. (1994) show that the transport deficit of lower NADW can be related to the climatological restoring data near the northern boundary; the use of actual section data that capture the hydrographic properties of the narrow core of overflow water leads to a downward shift in the core depth of the NADW flow and a significant enhancement in the net transports of mass and heat throughout the domain. Beckmann et al. (1994a) examine the effects of increasing the horizontal resolution (from $1/3°$ to $1/6°$), and report a trend toward smaller values of the mean meridional overturning, but little change in net heat transport. Böning et al. (1995) note that the basic CME cases, like many other large-scale circulation models, suffer from a spurious upwelling of deep water in the Gulf Stream region that has a deleterious effect on meridional overturning and heat transport in the lower latitudes.

This study builds on these previous analyses and furthers the original goals of the CME: to evaluate the performance of state-of-the-art ocean models through direct comparison with observations and to help guide future model development efforts. While the present paper focuses on the circulation and deep-water formation in the subpolar region, and the corresponding patterns of meridional overturning and heat transport in the North Atlantic, a companion paper (Bryan et al. 1995a) addresses the dynamics of the horizontal mass transport in the North Atlantic, including the interactions between the thermohaline-driven deep flows and bottom topography, and the mean circulation of the subtropical region.

In section 3 we discuss the three-dimensional flow patterns and water mass transformations in middle and higher latitudes for a basic, high-resolution model case with climatological forcing. In section 4 we use the host of CME experiments to examine the dependencies of the subpolar gyre circulation, deep-water formation, and meridional overturning on factors such as thermohaline forcing, horizontal resolution, and subgrid-scale mixing. Conclusions are given in section 5.

2. Model experiments

The basic model of the wind- and thermohaline-driven circulation is the primitive equation model developed by Bryan (1969) and Cox (1984). The CME configuration developed by Bryan and Holland (1989) spans the Atlantic Ocean from 15°S to 65°N. The computational domain includes the Caribbean Sea and Gulf of Mexico, but excludes the Mediterranean Sea. We shall use model versions with three different horizontal grids: a medium-resolution version with 1° by 1.2° (latitude by longitude), a high-resolution version with $1/3°$ by $2/5°$, and a very-high resolution version with $1/6°$ by $1/5°$. In all cases, there are 30 discrete levels in the vertical, with a spacing of 35 m at the surface, smoothly increasing to 250 m at 1000 m. Below 1000 m the vertical grid spacing is a constant 250 m. The experiments described in this paper are listed in Table 1.

There are several reasons for excluding the Nordic Seas from the model domain. First, to avoid an explicit simulation of the complex sequence of water mass transformations that lead to the formation of Arctic Intermediate Water and Norwegian Sea Water, the source waters for the outflows across the Greenland–Scotland Ridge. Second, to avoid the fundamental problems associated with a simulation of the overflow processes in numerical models that do not resolve the small Rossby radii over the ridge area (Gerdes 1993). Finally, to avoid the necessity of including an explicit simulation of sea ice formation and transport processes in the high northern latitudes. The position of the southern boundary at 15°S was chosen to avoid bisecting the subtropical gyre of the Southern Hemisphere. In the experiments described here, these boundaries are closed to inflow and outflow, but adjacent to them narrow "buffer" zones are introduced in which potential temperature θ and salinity S are damped toward observed values, thereby mimicking the water mass conversions that in reality take place in regions outside of the model domain. The width of the buffer zones is four grid boxes in all model versions, and the damping timescale decreases from 25 days in the grid box adjacent to the prognostic model interior to 5 days adjacent to the wall. The effect of the buffer zones and the efficiency and accuracy of the water mass conversions accomplished there, are examined with several sensitivity experiments. Similar buffer zones with a damping toward Levitus (1982) values of θ and S are introduced along the northern part of the continental shelf off Labrador (where otherwise an ice model would be necessary to prevent, e.g., the generation of supercooled water during winter) and near Gibraltar. The effect of the latter has been discussed elsewhere (Spall 1990; Beckmann et al. 1994a) and will not be of concern here.

Different schemes have been adopted for parameterization of subgrid-scale mixing of tracers and momentum. The eddy-resolving versions use a highly scale-selective, biharmonic diffusivity (A_h) and viscosity (A_m) for horizontal mixing. Different approaches were tested to parameterize the effect of eddy mixing on the resolved fields in the non-eddy-resolving version of the model. In the basic configuration, traditional Laplacian diffusion in the horizontal with constant coefficients was used. Other cases used the diffusion formulation described by Redi (1982), in the numerical implementation of Cox (1987), which is based on a rotation of the diffusive flux vector to a coordinate locally tangent to an isopycnal surface. The coefficients for along-isopycnal diffusivity are depth-dependent and vary between 2×10^7 cm^2 s^{-1} at the surface and 0.5×10^7 cm^2 s^{-1} at greater depth with an e-folding depth scale of 500 m. A small background horizontal diffusivity is necessary in this scheme to prevent numerical noise.

TABLE 1. List of CME experiments and model parameters relevant in the context of the present study. Vertical diffusivity is 0.3 $cm^2\ s^{-1}$ for all cases, vertical viscosity is 10 $cm^2\ s^{-1}$ except for N13-1 where it is 30 $cm^2\ s^{-1}$. Wind stresses are from the monthly mean climatologies of Hellerman and Rosenstein (1983, denoted HR) and Isemer and Hasse (1987, denoted IH). For horizontal mixing a biharmonic operator is used in the eddy-resolving version [units are $(-1)*10^{19}\ cm^4\ s^{-1}$], and a conventional Laplacian operator in the non-eddy-resolving version (units $10^7\ cm^2\ s^{-1}$), except for N1-26.0 which uses the Gent–McWilliams scheme with $\kappa = 1 \times 10^7\ cm^2\ s^{-1}$ and the K1-n cases which use the Redi scheme (see text). Experiment K1-NF is a sensitivity study where all surface buoyancy fluxes north of 47°N are turned off.

Expt.	Resolution ($\Delta\varphi \times \Delta\lambda$)	Mixing parameters A_m	A_h	Wind τ	Restoring data North	Restoring data South	Initial condition	Integration time (yr)
				(a) Eddy-resolving cases				
N13-1	1/3° × 0.4°	2.5	2.5	HR	Levitus	Levitus	Levitus	25
2	1/3° × 0.4°	1.0	1.0	HR	Levitus	Levitus	N13-1 at yr 20	5
K13-1	1/3° × 0.4°	2.5	2.5	HR	Levitus	Levitus	N13-1 at yr 16	8
2	1/3° × 0.4°	2.5	2.5	IH	Levitus	Levitus	K13-1 at yr 20	8
6	1/3° × 0.4°	2.5	2.5	IH	actual	Levitus	K13-4 at yr 33	21
7	1/3° × 0.4°	10.0	1.5	IH	actual	Levitus	K13-6 at yr 49	5
N16-1	1/6° × 0.2°	0.4	0.4	HR	Levitus	Levitus	N13-4 at yr 20	3
K16-1	1/6° × 0.2°	0.5	0.5	IH	Levitus	Levitus	K13-3 at yr 24	5
				(b) Non-eddy-resolving cases				
N1-12.0	1° × 1.2°	10	1	HR	Levitus	Levitus	Levitus	192
12.2	1° × 1.2°	10	1	HR	No restoring	Levitus	N1-12.0 at yr 61	157
12.3	1° × 1.2°	10	1	HR	Levitus	No restoring	N1-12.0 at yr 61	157
12.5	1° × 1.2°	10	1	1.3 × HR	Levitus	Levitus	N1-12.0 at yr 191	100
12.7	1° × 1.2°	10	1	No wind	Levitus	Levitus	N1-12.6 at yr 271	70[b]
25.0	1° × 1.2°	40	0.5	HR	Levitus	Levitus	N1-12.0 at yr 192	43
26.0	1° × 1.2°	G-M scheme		HR	Levitus	Levitus	N1-26.0 at yr 192	92
K1-C1	1° × 1.2°	Redi scheme		IH	Levitus	Levitus	Levitus	70
C2	1° × 1.2°	Redi scheme		IH	actual	Levitus	K1-C1 at yr 50	25
NF[a]	1° × 1.2°	Redi scheme		IH	Levitus	Levitus	K1-C1 at yr 50	25

[a] No surface buoyancy fluxes north of 47°N.
[b] Case N1-12.6 was initialized with N1-12.0 at yr 191, and used reduced wind stress (0.7 × HR).

One experiment is reported in which the parameterization of Gent and McWilliams (1990) is adopted. In addition to tracer diffusion along isopycnals as in the Redi scheme, there is an eddy-induced transport velocity in this scheme. Danabasoglu et al. (1994) discuss its effects on a coarsely resolved global ocean model.

The vertical mixing scheme is the same for all model cases, a second-order operator with constant coefficients for tracers (0.3 $cm^2\ s^{-1}$), and momentum (10 $cm^2\ s^{-1}$, except for N13-1 which used 30 $cm^2\ s^{-1}$), and an additional dissipation of momentum by a quadratic bottom drag. The effect of free convective overturning is parameterized by a convective adjustment scheme. In cases of static instability the vertical diffusion coefficient takes on a high value ($10^4\ cm^2\ s^{-1}$).

The thermohaline boundary conditions at the sea surface are based on seasonal climatological datasets. The thermal boundary condition is specified by a linear bulk formula. Following Haney (1971), the heat flux across the ocean surface is expressed as the difference between the model-predicted surface temperature and an "effective" atmospheric temperature T^*. The prescribed fields of the proportionality coefficient and of T^* were computed for each month from various climatological datasets as described by Han (1984). The proportionality coefficient varies temporally and spatially in the range 25–60 $W\ m^{-2}\ K^{-1}$, and is primarily a function of surface wind speed. For a derivation and plots of these fields we refer to Holland and Bryan (1994). The boundary condition for freshwater flux is implemented as a linear damping of salinity in the first model level toward the Levitus (1982) seasonal climatology.

The basic high-resolution case (N13-1) was initialized with January θ and S conditions taken from the Levitus (1982) climatology. The integration period for this first NCAR experiment was 25 years. All other 1/3° and 1/6° experiments were initialized with a solution from a previous experiment. The temporal evolution of the meridional overturning to changes in the thermohaline forcing near the northern boundary was examined by Döscher et al. (1994), showing an adjustment to a quasi-dynamic equilibrium within 10–15 years. Similar results, for a different North Atlantic model, are reported by Gerdes and Köberle (1995). Both the basic case and its variants with buffer zone restoring to Levitus data and the two Kiel cases with northern buffer zone restoring to actual section data can be considered to be in quasi-dynamic equilibrium; the integration time for both versions has been longer than

20 years. The model variants with different mixing coefficients have been integrated for shorter periods of time. In these cases, there are only negligible tendencies in the large-scale circulation patterns, except for case K13-7 where the ratio of viscosity to diffusivity is increased as an attempt to reduce the artificial upwelling in the Gulf Stream regime. Longer integration periods could be afforded for the 1° version of the model, but were, in most cases, of little consequence for the large-scale transport patterns that are the primary concern of the present study.

3. Mean circulation patterns: Basic case

Before exploring the dependencies on forcing schemes and model factors in section 4, we will examine in somewhat more detail the three-dimensional circulation for a standard 1/3° case with climatological restoring conditions at the northern and southern boundaries. The description is mainly based on N13-1, but there are only little differences to the other NCAR cases (N13-*n*) and the Kiel cases (K13-1 to -5) with these boundary conditions.

a. Meridional overturning

The long-term mean, zonally integrated volume transport for the 1/3° model is presented in two ways: Figure 1a shows the streamfunction $\phi(\varphi, z)$ in the latitude–depth plane, and Fig. 1b shows the streamfunction as a function of latitude and potential temperature, $\phi^*(\varphi, \theta)$ (for a definition, see Bryan and Sarmiento 1985). The streamfunction in the latitude-depth plane exhibits the familiar pattern of shallow overturning cells associated with the divergence (at the equator) and convergence (near 30°N) of the wind-driven currents at the surface. The depth of these cells is 200 m in the equatorial Atlantic, and about 400 m in the midlatitudes. As discussed by Bryan et al. (1995b) for the tropical and Bryan et al. (1995a) for the midlatitude Atlantic, the wind-driven transports vary substantially between model cases forced with different climatologies. However, the differences in the wind-driven cells have only little effect on the strength of the two deep overturning cells associated with the formation and southward flow of NADW and with the northward flow of AABW; the results shown in Fig. 1 are, therefore, fairly representative for all 1/3° cases using the climatological relaxation conditions at the northern and southern boundaries. The maximum of the NADW cell of about 12 Sv is found near 47°N, at about 1000-m depth. The southward transport of NADW is augmented by an upwelling of bottom water imported from the South Atlantic; the cross-equatorial transport in the basic case is about 5 Sv.

A striking feature of the overturning pattern is the strong upwelling of deep water taking place in the midlatitudes, especially between 30° and 40°N. Only a third of the deep water formed in the subpolar North Atlantic finds its way across the equator, to be transformed to upper intermediate and thermocline water in the restoring zone at the southern boundary. This model pattern stands in contrast to the observational picture as summarized by Schmitz and McCartney (1993). In their account, the formation rate of "new" NADW in the subpolar North Atlantic is about 13–14 Sv, commensurate with the northward flow of intermediate water across 32°S (Rintoul 1991) and of water of South Atlantic origin through the Straits of Florida (Schmitz and Richardson 1991). This estimate is somewhat lower than the meridional transport (17 Sv) inferred from the zonal, transoceanic sections at 36° and 25°N by RW. On the whole, the observations do not indicate a significant net upwelling (in the zonally integrated sense) of NADW in midlatitudes as seen in the model solution.

Figure 1b indicates a monotonic cooling of the northward flowing surface water, as a result of the upper thermal boundary condition. There is a transport of about 20 Sv of warm North Atlantic water across 55°N. The cooling in the subpolar ocean produces a water mass in a rather narrow temperature range, 3°–4°C (Upper NADW). All of the southward transport is concentrated in this temperature range. In the subpolar North Atlantic, the recirculation takes place partly in the deep ocean (Fig. 1a) and partly horizontally in the subpolar gyre. The lack of production and southward transport of water with temperature less than 3°C (Lower NADW) corresponds to a rather small vertical penetration of the NADW cell. In the basic model case presented here it does not extend beneath 2000–2500 m (Fig. 1a), in contrast to the vertical profiles of meridional transport that had been inferred from zonal hydrographic sections in the subtropical North Atlantic (HB, RW).

b. Upper-layer circulation in the subpolar North Atlantic

The most prominent feature of the upper-layer flow field in the high-resolution model cases is the band of energetic eddies straddling the course of the North Atlantic Current (NAC) (Figs. 2a,b). Both model and observations indicate a sharp drop of eddy kinetic energy from its maximum in the Newfoundland Basin across the Subpolar Front to the northwest (Krauss and Käse 1984; Beckmann et al. 1994b). In the mean fields of velocity (Fig. 2c), temperature (Fig. 3a), and salinity (Fig. 3b), the Subpolar Front to the west of 40°W stands out as a remarkably sharp feature, corresponding to a rather stable course, and little meandering of the NAC in the "Northwest Corner," and indicative of small cross-frontal mixing in this area.

The position of the Subpolar Front and course of the NAC depend on a number of model factors. While increasing the resolution beyond 1/3° seems to have com-

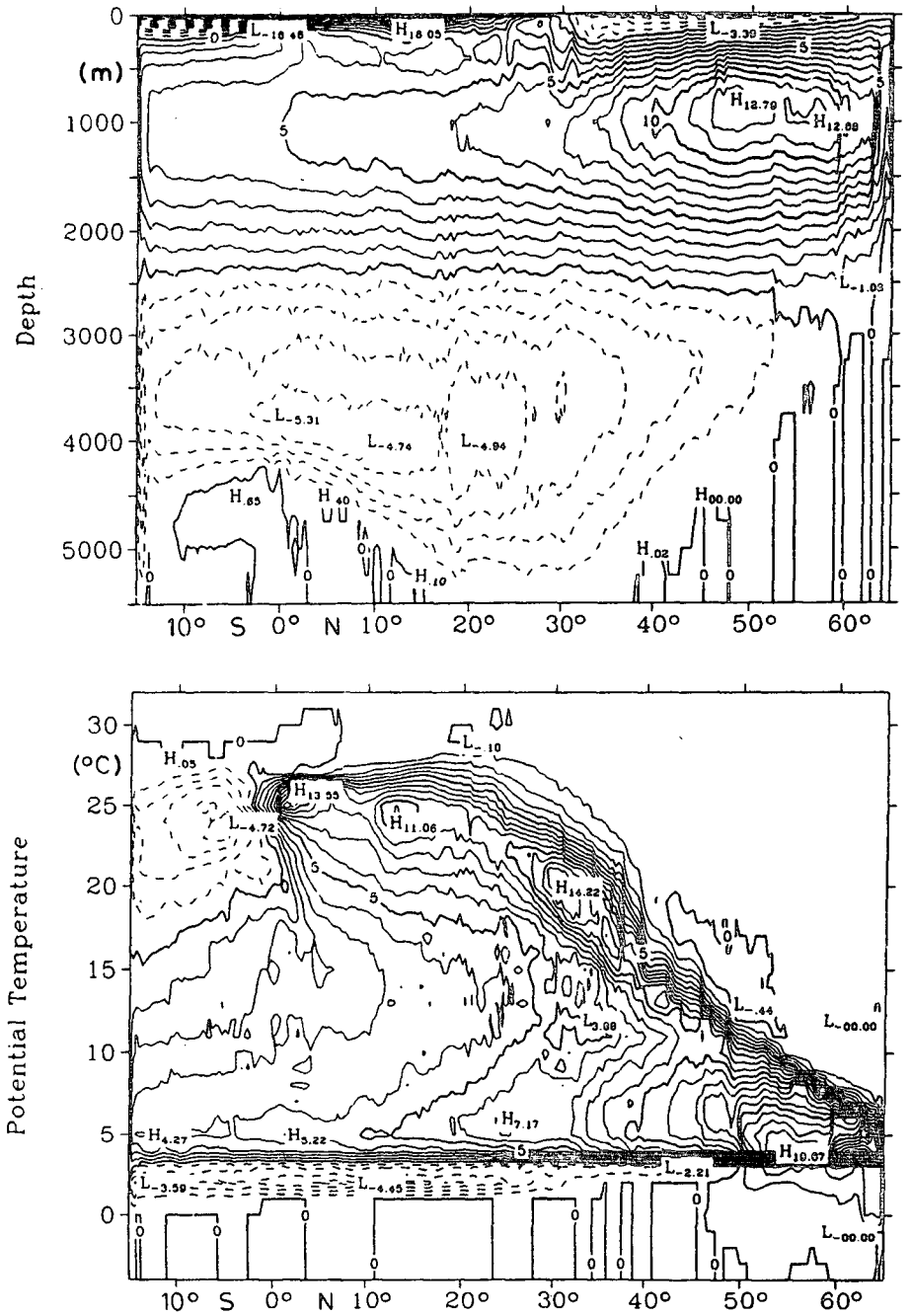

FIG. 1. Streamfunction (in Sv, 1 Sv $\equiv 10^6$ m^3 s^{-1}) of the zonally integrated, time-mean flow (averaged over 5 years) (a) in the latitude–depth plane, (b) in the latitude–potential temperature plane; for the basic case N13-1.

paratively little influence on the mean fields, there is a significant difference between the non-eddy-resolving (1°) and the eddy-resolving (1/3° and 1/6°) cases in the Newfoundland Basin. The Subpolar Front in the eddy-resolving cases is not only sharper than in the 1° model but also shifted to the north, leading to higher, and more realistic, sea surface temperatures over a large area of the Newfoundland Basin.

An unrealistic feature of the mean surface current field in the high-resolution cases as shown in Fig. 2c concerns the path of the northward flow along the Grand Banks: the current is pressed against the conti-

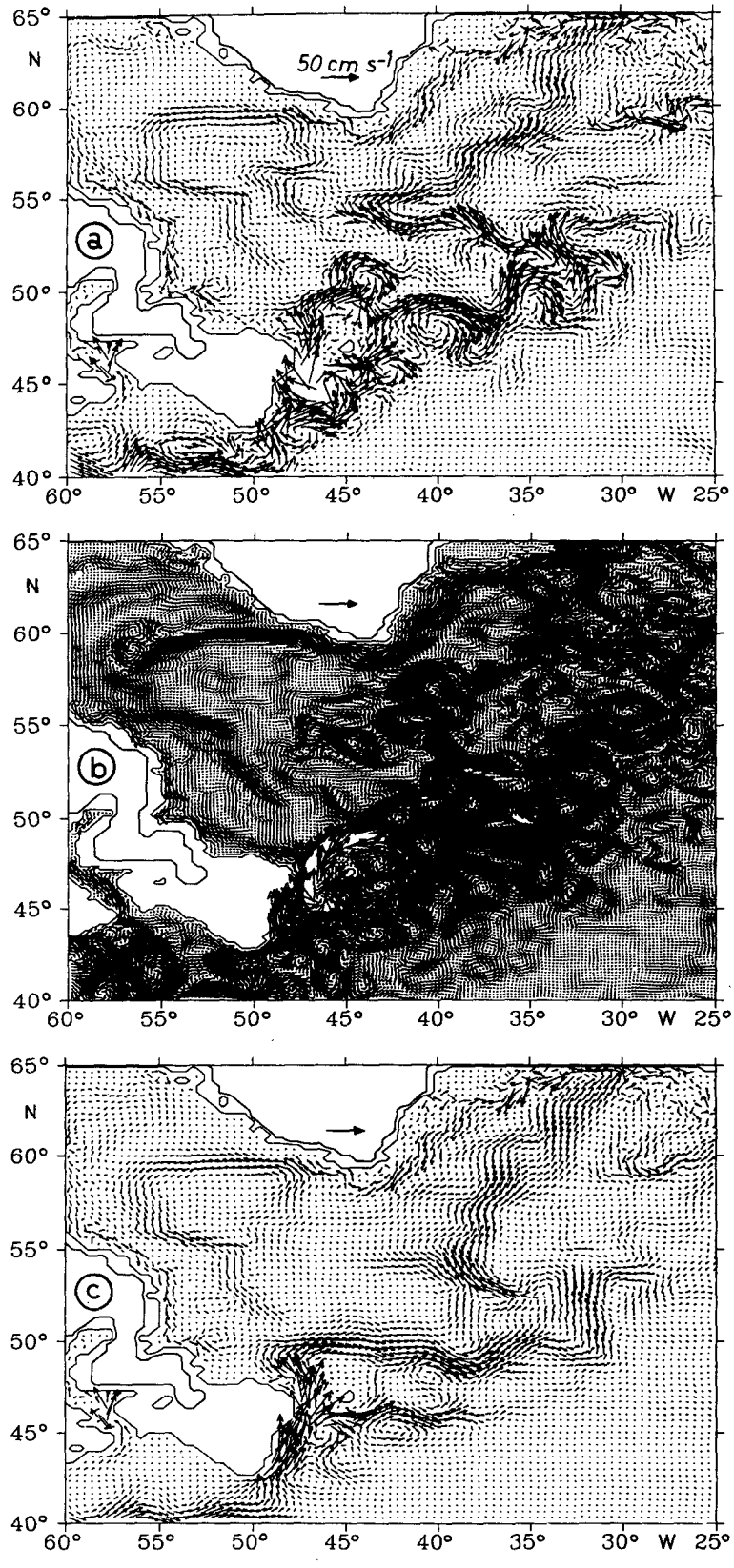

FIG. 2. Horizontal velocity fields in the upper layer (depth 180 m). Snapshots (a) of the 1/3° model (N13-1) and (b) of the 1/6° model (N16-1), and (c) 5-year mean flow for the 1/3° model.

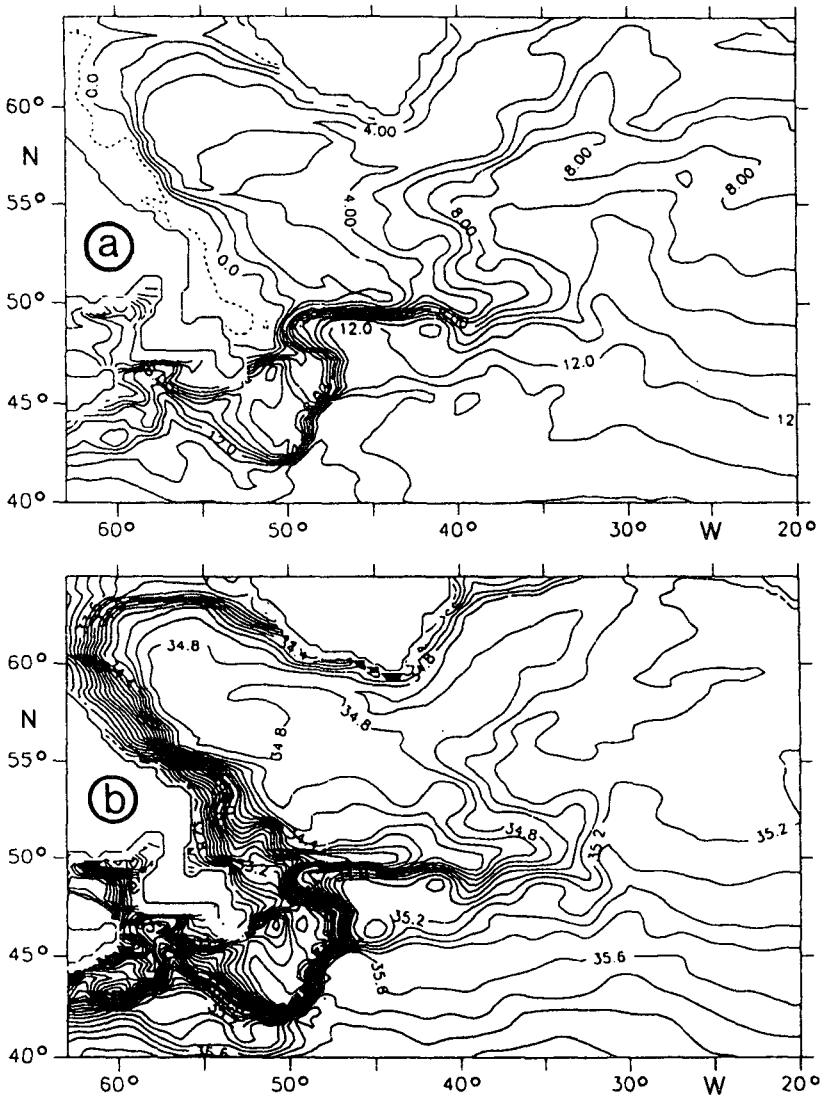

FIG. 3. (a) Mean potential temperature (CI = 1°C) and (b) salinity (CI = 0.1) at 91-m depth in winter (Jan–Feb–Mar) for the 1/3° basic model.

nental slope with the bulk of the water carried through Flemish Pass instead of flowing to the east of Flemish Cap as observed. Possibly related to that, the Labrador Current is blocked at the northern edge of the Grand Banks and a wedge of cold fresh Labrador shelf water is drawn eastward along the Subpolar Front (Fig. 3). The dynamical cause of this local model problem is not clear. It characterizes not only all high-resolution cases of the CME (both the 1/3° and the 1/6° version), but can be seen also in the solution of the 1/2° World Ocean model of Semtner and Chervin (1992), and thus seems to be a rather robust feature of the GFDL model in this area.

The course of the NAC farther downstream is strongly affected by the conditions applied at the artificial northern boundary of the model. In the high-resolution cases with a closed boundary at 65°N the bulk of the NAC turns northward already by about 35°W, leaving the northeastern basin somewhat too cold and far too quiescent. Because the buffer zone in the high-resolution cases does not extend south of Iceland, in order to satisfy mass conservation upper-layer water must be drawn into the buffer zone between Greenland and Iceland to be converted to Denmark Strait overflow water (DSOW), rather than to the east of Iceland. The horizontal mass transport in the subpolar gyre and its dependence on the surface forcing and the northern boundary condition will be examined more closely in section 4b.

c. Deep-water formation

The water mass transformation due to surface cooling during winter is illustrated in Fig. 4, showing the depth and the temperature of the mixed layer in a similar fashion as in the observational study of McCartney and Talley (1982). They demonstrate that continuous cooling along the NAC and the cyclonic circulation in the subpolar North Atlantic form a progression of pycnostads (subpolar mode water), the coldest being the Labrador Sea Water (LSW) with temperatures below 3.5°C. The major patterns of the observed fields are reproduced by the model solution: a broad band of increasing mixed layer depths extends in an east-northeastward direction across the Atlantic and along the cyclonic flow in the subpolar gyre (with a minimum depth of the homogenized layer, as in the observations, along the axis of the NAC in the Newfoundland Basin). The mixed layer temperatures smoothly decrease downstream to reach a minimum of about 3°C in the Labrador Sea near 58°N, 50°W. The minimum temperature coincides with a maximum thickness (>2000 m) of the homogenized layer in late winter.

Cross sections along 58°N in late winter (Fig. 5) exhibit the cyclonic circulation of the Labrador Sea and the homogenized water near the center of the gyre. The gross hydrographic properties are in fair agreement with the observations of Clarke and Gascard (1983) who found a nearly homogeneous body of water to depths greater than 2000 m in the area 56°–57°N, 53°–56°W within a cyclonic gyre of diameter 200–400 km. The observed potential temperatures were about 2.9°C, salinities close to 34.84 psu, and potential densities about 27.78. Their estimate of the volume of LSW formed during a winter (based on all the water found within the cyclonic gyre above the pycnocline) was 1.2×10^5 km^3. Averaging this production over a year, Clarke and Gascard (1983) estimated an equivalent transport of 3.9 Sv. Over the final winter of the model integration, the volume of water in the range $2.6°C < \theta < 3.0°C$, $34.7 < S < 34.9$ psu increases from a minimum of 0.25×10^5 km^3 in November to a maximum of 1.34×10^5 km^3 in April. Hence, the production of water in this θ–S class during the final winter of the simulation is 1.1×10^5 km^3, corresponding to an equivalent annual production of 3.5 Sv, close to the estimate of Clarke and Gascard (1983). The total volume of water within the Labrador Sea that is involved in convection, that is, points undergoing convective adjustment, is actually larger: 5.5×10^5 km^3, reaching a maximum in March. However, these quantities are variable from year to year, even with a repeating annual-cycle surface forcing. The volume of water in the θ–S range defined above in March varies from a low of 1.03×10^5 km^3 to a maximum of 1.47×10^5 km^3 over the last five years of the experiment. In the following, we shall examine the effect of the water mass transformation in the Labrador Sea on the net production and export of NADW from the subpolar North Atlantic.

Figure 6 shows box budgets of mass transport for the upper layer (0–1000 m) north of 30°N and indicates schematically the main pathways of the water that flows northward with the Gulf Stream and its extension, the NAC. In the basic high-resolution case (N13-2), the net northward flow of upper-layer water across 47°N, primarily carried by the NAC, is 12.5 Sv. As pointed out earlier, this appears only slightly weaker than the total warm to cold water conversion according to the observational scheme of Schmitz and McCartney (1993). Farther north, the NAC transport is higher because of the recirculation in the subpolar gyre; for example, the northward transport of warm and salty water across 55°N is about 20 Sv, as may be seen in Fig. 1b. Observed geostrophic transports of the NAC into the northeastern Atlantic are 21.6 Sv (across 53.5°N) (Krauss 1986), and 18 Sv (Saunders 1982). The synthesized circulation scheme of Schmitz and McCartney (1993) suggests a total northward transport of 20 Sv for water with $\theta > 7°C$, which includes a component recirculating in the subpolar gyre of 7 Sv.

The downwelling of the 12.5 Sv imported by the NAC in the model occurs predominantly in the northeastern parts of the basin. There is a vertical transport of 4.3 Sv at 1000 m in the northern buffer zone, but an even larger amount of sinking takes place south of it, mostly in the Iceland Basin. (It should be noted that "sinking" as defined here does not imply the presence of localized columns with vertical flow. What we consider are integral effects over more or less extended areas. Interestingly, downward motion is found mainly close to topographic features, such as the continental slope south of Iceland, and the Reykjanes Ridge—that is, areas where we usually also find boundary currents. The situation may be pictured in the form of quasi-horizontal currents, weakly inclined against the isobaths.) Despite that the deepest winter convection occurs in the Labrador Sea, the mean vertical transport there is only about 1 Sv, much smaller than the rate inferred from the volume of homogenized water produced in the area.

d. Circulation of deep and bottom water

The mean flow in the deep subpolar North Atlantic is shown in Fig. 7. An intense deep boundary current (DBC) originates along the East Greenland continental slope, and flows cyclonically around the Labrador Basin. Typical velocities are 10–15 cm s^{-1}, with maxima of 20–25 cm s^{-1} east of Greenland, and 15–20 cm s^{-1} off Labrador. The DBC forming in the Irminger and Labrador Basin does not continue along the western boundary in the Newfoundland Basin. Instead, the current is deflected eastward at about 51°N, just to the north of the overlying Subpolar Front. A similar deep flow structure, with an anticyclonic circulation in the

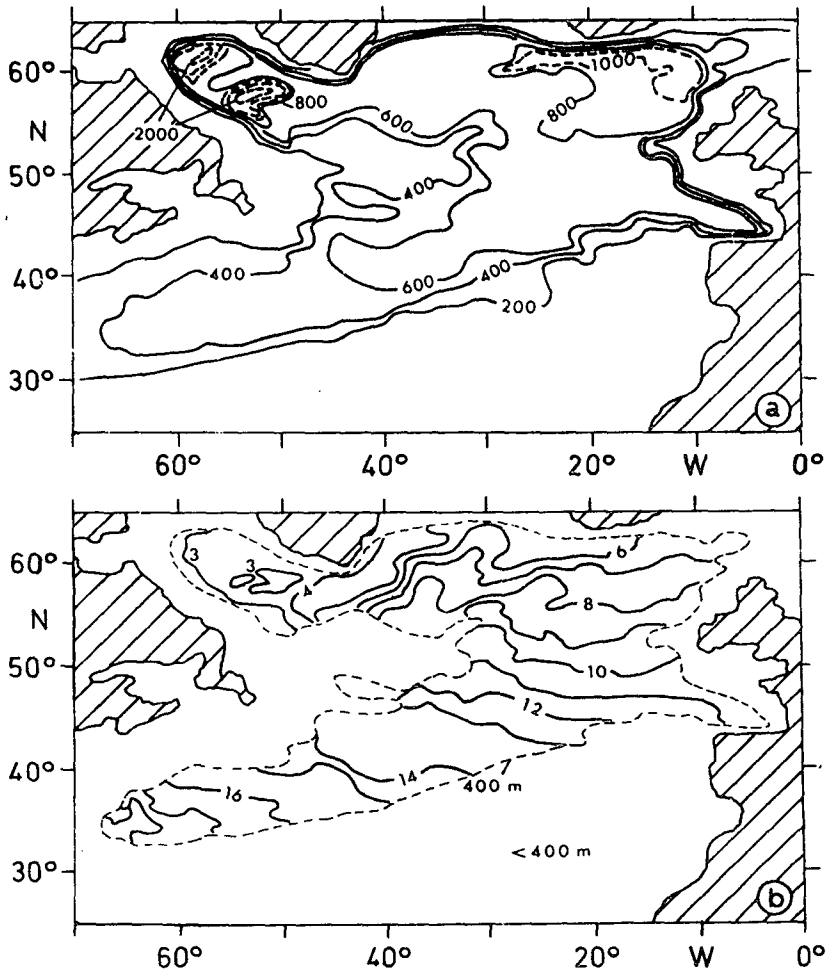

FIG. 4. (a) Depth of the surface mixed layer in late winter (day 91) for the basic 1/3° case, defined in analogy to McCartney and Talley (1982) by a potential density interval of 0.02 mg cm^{-3}. (b) Potential temperature of the surface layer, contoured only where layer depths exceed 400 m.

Newfoundland Basin, characterizes all CME models, regardless of resolution. It may be interesting to note that a similar pattern can be seen in other simulations with medium- to high-resolution models such as Gerdes (1988) or Semtner and Chervin (1992), indicating a rather robust model behavior.

Figure 8 shows box budgets of the mass transport in the model layers 1000–3500 m. The deep-water production in the northeastern parts of the basin leads to a westward transport around Cape Farewell of 9.3 Sv. (The total, vertically integrated transport of the northern boundary current between the Cape and 57°N is 20 Sv.) There is some enhancement of the deep boundary current due to sinking of upper-layer water in the Labrador and Newfoundland Basins (net 0.9 Sv), near the Mid-Atlantic Ridge (0.8 Sv), and due to upwelling of bottom water (1.4 Sv) that (together with some westward flow across the Mid-Atlantic Ridge south of the main pathway) yield a net deep-water export across 47°N of 13.8 Sv. The outflow takes place almost exclusively in the western basin. The box budgets reveal that the midlatitude upwelling pattern seen in the meridional overturning (Fig. 1a), is concentrated in the two western boxes (5.7 Sv), whereas vertical fluxes in the interior are small.

Though several authors have advanced schemes for the water mass renewal and circulation, there are only a few direct measurements of the transport in the subpolar North Atlantic that may be used for a quantitative test of the model solution. Dickson et al. (1991) obtained a mean transport of 10.7 Sv for the dense ($\sigma > 27.8$) waters flowing south along the continental slope off eastern Greenland near 63°N, which appeared consistent with the estimate of Clarke (1984) for the flow of deep and bottom waters around Cape Farewell (13.3 Sv, according to the recalculation presented in

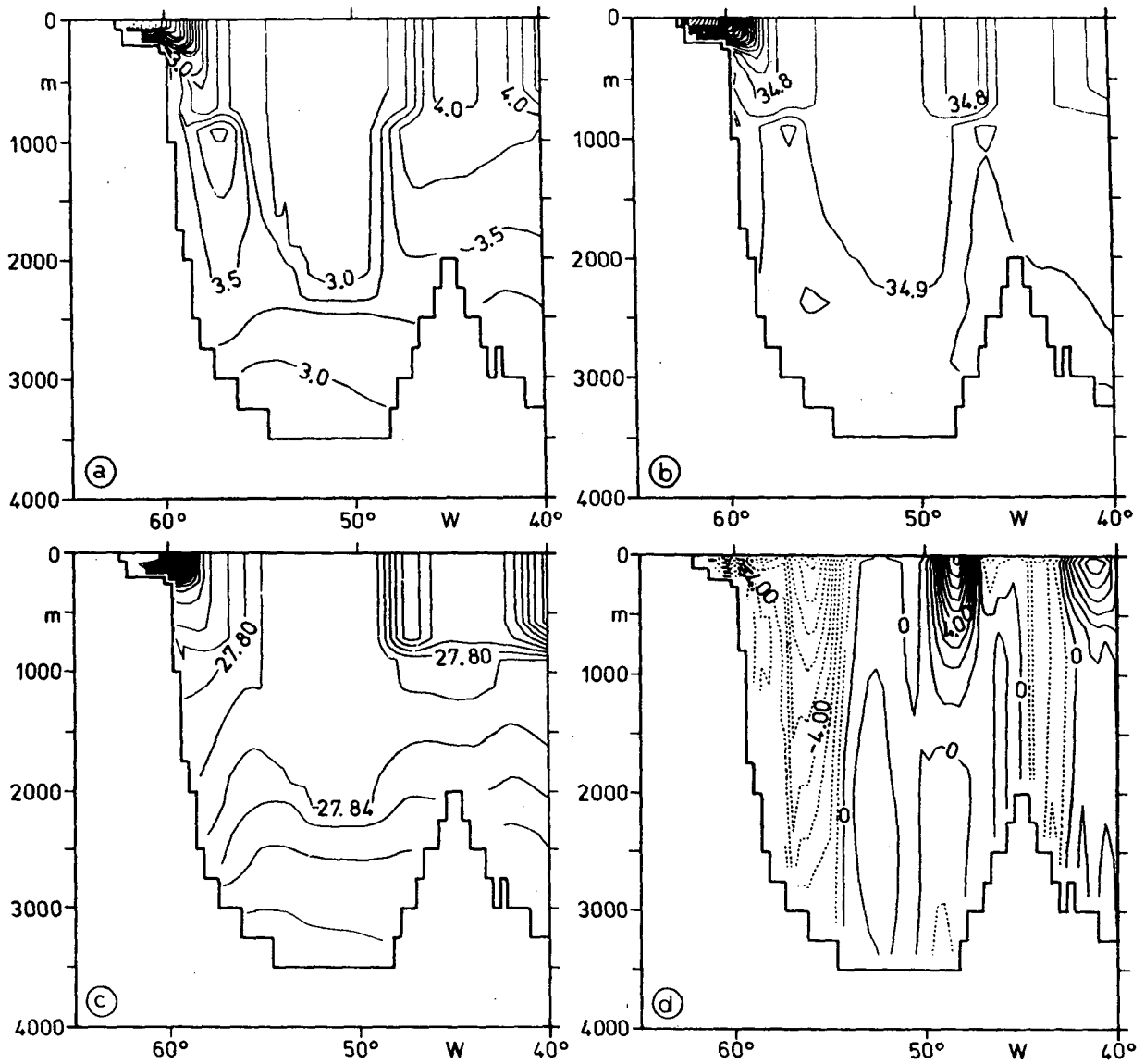

FIG. 5. Zonal cross sections along 58°N in late winter (day 91) for the basic 1/3° case. (a) Potential temperature (CI = 0.25°C), (b) salinity (CI = 0.05), (c) potential density (CI = 0.02), (d) meridional velocity (CI = 1 cm s^{-1}).

Dickson et al. 1991), indicating some further enhancement due to entrainment. Adding the estimate of Clarke (1984) for the transport of recirculating Labrador Sea Water (3.5 Sv), the total transport of deep water around Cape Farewell is about 17 Sv. The deep-layer transport in the basic model case is considerably smaller at this site, indicating a lack of horizontal recirculation of deep water in the Labrador/Irminger Basin. The factors governing the deep-water formation rate and subpolar circulation will be examined in sections 4a and 4b.

Figure 9 shows the mass transport budgets for the layer 3500–5500 m. The northward flow of AABW across the equator is about 5 Sv in this model case (see Fig. 1a), almost entirely in the western basin. While this is in accordance with the estimate of McCartney and Curry (1993), almost none of the model AABW invades the eastern basin, in contrast to the observational evidence for flow of about 2 Sv through the Vema Fracture Zone at 11°N (McCartney et al. 1991). A possible reason is that the relevant fracture zones in the Mid-Atlantic Ridge might not be well enough resolved in the model. The northward flow of AABW across 30°N is 4 Sv. While there is only little upwelling and mixing with the overlying deep water between the equator and this latitude, there is a continuous loss of bottom water transport through gradual upwelling along its northward flow path; only 1.4 Sv make it into

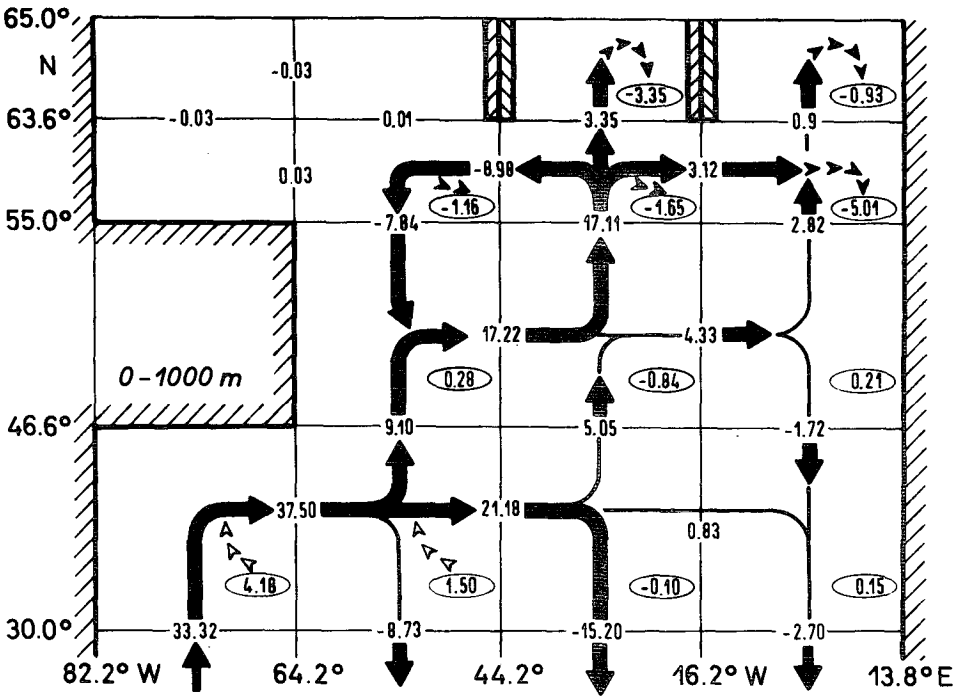

FIG. 6. Mass balance for the layer 0–1000 m in the basic 1/3° model. Numbers in the lower right hand corner of each box denote vertical transport (Sv) at 1000 m; negative values represent sinking, positive upwelling. Numbers at the box boundaries denote horizontal transports. For illustration, the main pathways of the 3D circulation are schematically indicated.

the subpolar North Atlantic across 47°N, compared to 3 Sv in the observational account of McCartney (1992) and Schmitz and McCartney (1993) (of which 2 Sv are supposed to enter in the eastern basin).

4. Sensitivity studies

In this section we shall use results from the large number of CME experiments to examine the sensitivities of the main processes and circulation elements that determine the location and rate of deep-water production (section 4a), the mass transport in the subpolar gyre (section 4b), and the strength and structure of the meridional overturning circulation and associated heat transport in the basin (section 4c).

a. Deep-water production

Table 2 gives a compilation of the horizontal and vertical volume transports through some key sections in the subpolar North Atlantic from model cases with different horizontal resolution, mixing parameters, wind forcing, and thermohaline forcing. The sections are defined on the basis of the box budgets shown in Fig. 6; however, for simplification some of the individual boxes have been combined here. To assess the location and rate of deep-water production in the different model cases, we will consider the net sinking north of 47°N, across the 1000-m depth and its partitioning in three main areas: the Labrador/Newfoundland Basin west of 44°W, the Irminger and Iceland Basins, and the northern buffer zone. The geographical division between the latter two areas differs between the eddy- and non-eddy-resolving versions of the model since the buffer zone encompasses four grid boxes in each version. In almost all model cases, the net sinking north of 47°N is close to the maximum of the zonally integrated streamfunction as displayed in Fig. 1a. The total export of deep water across 47°N is represented by the sum of the sinking of upper-layer water and the upwelling of bottom water. The upwelling is given for the depth (which is highly variable between different model cases as we will see in section 4b) that separates the northward flowing bottom water and southward flowing deep water. The net sinking of upper-layer water, upwelling of bottom water, and net export of deep water may be compared with the observationally based estimates put forward in the circulation scheme of Schmitz and McCartney (1993), that is, 13, 3, and 16 Sv.

The most robust model feature as depicted in Table 2 is the very small contribution of the Labrador Sea to the overall deep-water production and overturning. In all model cases, the sinking of surface water is concentrated in two areas: the artificial buffer zone to the east of Greenland, and the northeastern Atlantic, south of

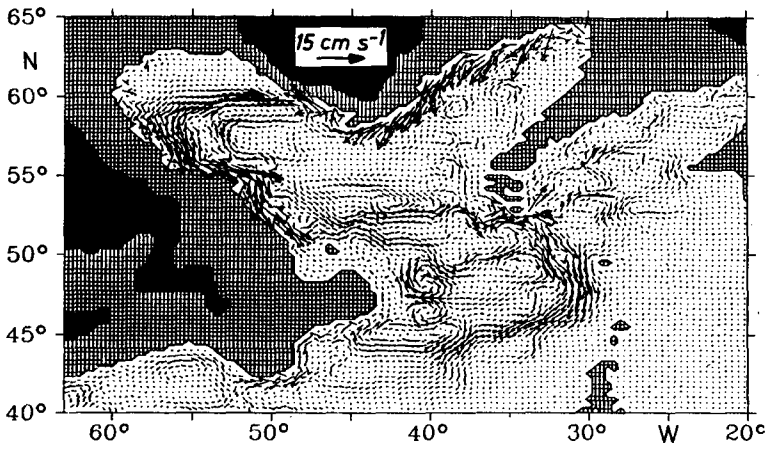

FIG. 7. Mean flow at 2125 m depth in the 1/3° basic case.

Iceland. The large-scale dynamical effect of the water mass modification by the deep winter convection in the Labrador Sea appears negligible. Even a complete shutdown of the deep convection, as in case K1-NF where the surface heat and freshwater fluxes over the whole subpolar North Atlantic north of 45°N were turned off, has little effect on the net sinking and meridional overturning in the basin or the partitioning among regions of the vertical transport across 1000 m compared to the reference case K1-C1.

The role of the northern buffer zone in the forcing of the meridional overturning can be deduced by comparing different model cases. Without any restoring of θ and S in the 1° model (N1-12.2), the vertical transport in that region decreases to 9.7 from 13.9 Sv in the reference case with climatological restoring data (N1-

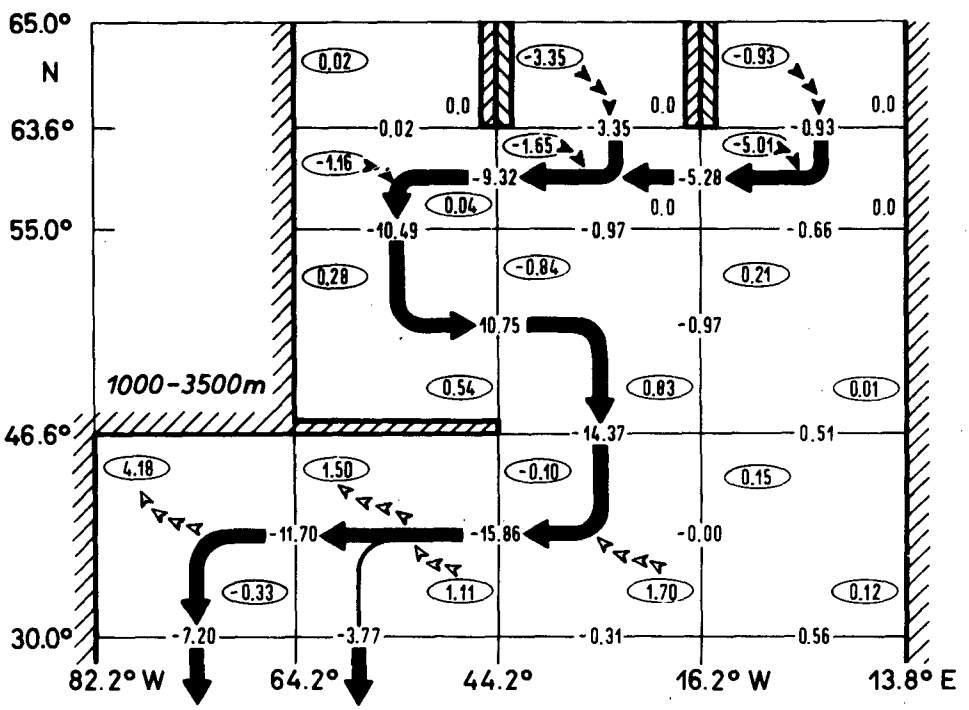

FIG. 8. Mass balance for the layer 1000–3500 m in the basic 1/3° model. Numbers in the upper left hand corners denote vertical transport at 1000 m, in the lower right hand corners denote vertical transport at 3500 m.

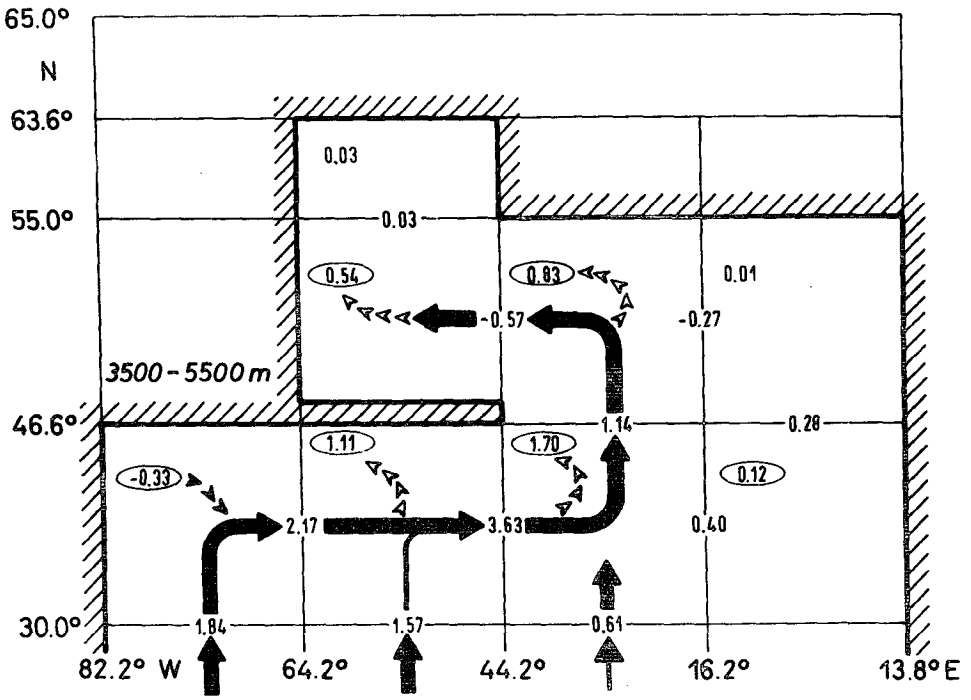

FIG. 9. Mass balance for the layer 3500 m–bottom in the basic 1/3° model. Numbers in the upper left corner denote vertical transport at 3500 m. Schematic representation of the main flow pathways as in Figs. 8 and 12.

12.0). Corresponding to that, the maximum of the zonally integrated streamfunction (meridional overturning) in the basin decreases from 16.6 to 11.8 Sv. Hence, the net effect of climatological restoring in the northern buffer zone of the 1° model version is 3–4 Sv. This roughly corresponds to the total sinking found in the narrower buffer zones of the high-resolution cases. One can assume that the net effect of restoring to climatological data in the high-resolution cases is smaller because the vertical transports in the buffer zone represent the sum of the restoring effect and the sinking that would take place without any restoring. Less effective buffer zones in the high-resolution cases probably have to be regarded as the principal cause of the smaller net overturning rates that are obtained in the 1/3° and 1/6° models.

As shown in Döscher et al. (1994), the hydrographic signature of Denmark Strait overflow water (DSOW), which is spilled out through Denmark Strait and flows south in a narrow current adjacent to the continental slope of Greenland, is not captured in the smoothed climatological dataset of Levitus (1982). A restoring to θ and S values based on actual section data that include the DSOW core lead to a roughly 4 Sv higher deep-water production in the buffer zones of both the coarse- and the high-resolution model (K1-C2 and K13-6, respectively).

A contribution due to an influx of AABW to the net southward export of NADW can be identified in nearly all CME solutions (Table 2). In most cases the AABW transport across 47°N is smaller than the observational estimate of 3 Sv. Only some cases reach or exceed this value (K13-3 with 3.5 Sv and K16-1 with 3.9 Sv are not included in Table 2). A stronger northward flux of AABW usually comes at the expense of a decreased net renewal of NADW (and vice versa), reflecting some interrelation between the strength of the NADW and AABW overturning cells (we will come back to this in the following section). A notable exception is the 1/3° case with restoring to actual section data (K13-6), in which both the net sinking (15.0 Sv) and the upwelling (3.5 Sv) slightly exceed the observational numbers, yielding a total outflow of deep water of 18.5 Sv. Several 1° model versions also reach or exceed the observational estimate of 16 Sv (Schmitz and Cartney 1993) for the total NADW production, usually due to a stronger sinking, while the AABW contribution remains comparatively small: the cases with climatological restoring (N1-12.0, N1-25.0, K1-C1) give total deep-water transports between 15.6 and 16.9 Sv, the case with restoring to actual section data (K1-C2) 20.0 Sv.

b. Mass transport in the subpolar gyre

In Table 3 we have compiled the westward transports of the northern boundary current around Cape Farewell (44°W), for the layers 0–1000 m and 1000 m–bottom,

TABLE 2. Production of North Atlantic Deep Water north of 47°N for selected model cases. Sinking of upper-layer water across 1000 m is given (in Sv) for three different areas, defined as a subset of the boxes shown in Fig. 6: area (2) comprises the northeastern boxes east of 44.2°W, area (3) the Labrador and Newfoundland Seas west of 44.2°W; the width of the buffer zone (1) adjacent to the northern boundary east of Greenland is 4° in the coarse- and 4/3° in the high-resolution cases. The total sinking (1) + (2) + (3) is close to the maximum of the NADW overturning cell at 47°N (4); a small difference can result if that maximum is not exactly at 1000-m depth. The magnitude of the AABW cell at 47°N (5) gives the upwelling of bottom water north of that latitude. The net southward transport of NADW across 47°N is given by the sum of the sinking of upper-layer water (4) and upwelling of bottom water (5).

		Sinking			NADW cell at 47°N	AABW cell	NADW transport at 47°N
Case	Grid $\Delta\varphi$ (°lat)	Buffer zone (1)	NE Atlantic (2)	Labrador Sea (3)	(4) ≈ (1) + (2) + (3)	(5)	(4) + (5)
				(a) Resolution			
N1-12.0	1°	13.9	2.2	0.5	16.6	0.3	16.9
N13-1	1/3°	4.3	7.3	0.9	12.5	1.3	13.8
N16-1	1/6°	5.7	4.0	1.3	11.7	1.9	13.6[c]
				(b) Mixing parameterization			
N1-25.0	1°	13.8	1.6	−0.4[b]	15.3	0.3	15.6
K1-C1	1°	13.1	2.9	0.4	16.3	0.6	16.9
N1-26.0	1°	12.7	3.0	0.9	16.5	0.0	16.5
				(c) Wind stress			
N1-12.7 No wind	1°	16.6	2.6	0.8	20.2	0.3	20.5
N1-12.5 Stronger wind	1°	13.2	1.8	0.5	15.5	0.3	15.8
				(d) Thermohaline forcing			
N1-12.2 N:restoring off	1°	9.7[a]	0.4	1.0	11.8	1.4	13.2
N1-12.3 S:restoring off	1°	8.4	0.3	0.0	8.8	0.1	8.9
K1-C2 N:actual section	1°	18.0	0.1	1.0	20.0	0.0	20.0
K13-6 N:actual section	1/3°	7.9	7.0	−0.3[b]	15.0	3.5	18.5
K1-NF Sfc flux off	1°	13.2	2.4	0.2	15.8	0.5	16.3

[a] No restoring in northern buffer zone.
[b] Negative value: upwelling.
[c] These numbers are for a 1-year mean only. The streamfunction is rather noisy at 47°N.

for a number of model cases that allow an examination of the effects of wind- and thermohaline-forcing. Because of the different widths of the boundary currents in the high- and low-resolution versions, the westward transports are taken between Cape Farewell and 57°N in the former and between Cape Farewell and 55°N in the latter cases. The boundary current transports may be compared with the observational estimates of Clarke (1984). For the upper layers, he gives a westward transport of 14 Sv, reflecting the cyclonic recirculation (Irminger Current) of the waters carried northward by the NAC, and a contribution of 3 Sv from the shallow East Greenland Current that carries cold and fresh waters of Arctic origin. For the deep layers comprising the

TABLE 3. Influence of wind and thermohaline forcing on the transport of the subpolar gyre at Cape Farewell. The westward mass transport of the northern boundary current at 44°N is taken between Cape Farewell and 55°N in the coarse- and 57°N in the high-resolution cases. (In Sv)

Case		$\Delta\varphi$ (°lat)	0–1000 m	1000 m–bottom	Total
N1-12.0		1	7.6	12.5	20.1
N13-1		1/3	10.3	9.7	20.0
N1-12.07	No wind	1	1.8	13.2	15.0
N1-12.5	Strong wind	1	8.7	12.5	21.2
N1-12.2	N: restoring off	1	1.4	−0.1	1.3
K1-C2	N: actual section	1	8.5	26.1	34.6
K13-6	N: actual section	1/3	12.4	15.7	28.1
K1-NF	Sfc. flux off	1	9.3	11.9	21.2

overflow waters and recirculating LSW, the mass transport estimate is 17 Sv. Note that Schmitz and McCartney (1993) give higher transports for the deep water, mainly because of a higher estimate for the recirculation of Labrador Sea Water in the subpolar North Atlantic.

An important result revealed by an intercomparison of the DBC transports in the different model cases is the weak dependence on the wind forcing. Increasing the wind stress by a factor of 1.3 (N1-12.5) has little effect on the mean horizontal transport, it only increases from 20.1 to 21.2 Sv. Even a complete turn-off of the wind forcing (N1-12.7) results in only a 25% decrease in the vertically integrated transport at Cape Farewell (from a sharp drop in the upper-layer transport). The comparatively small sensitivity is in accordance with the analysis of the vorticity balance of the time-mean horizontal mass transport presented in Bryan et al. (1995a): linear vorticity dynamics, including the effects of bottom torques, cannot explain the transport pattern in the subpolar region. The model transports across 44°W bear little resemblence to those predicted by the Sverdrup relation, which would give about 40 Sv for the climatologies of HR and IH. Note, however, that all these considerations only apply for the time-mean transport, not for its wind-driven seasonal variation.

Thermohaline forcing, especially the formulation of the northern boundary condition, exerts a much stronger control on the volume transport in the subpolar gyre. A turn-off of the restoring (N1-12.2) causes a dramatic weakening of the gyre transport; the flow around Cape Farewell almost vanishes, both in the surface and in the deep layer. On the other hand, the use of actual section data for the buffer zone (cases K1-C2 and K13-6) leads to a significant increase of the deep-water transport around Cape Farewell (giving total transports of 34.6 and 28.1 Sv, respectively), apparently bringing its value closer to the observational estimates. On the other hand, there is almost no effect on the horizontal gyre transport in case K1-NF where the thermohaline fluxes at the surface were turned off (which did not affect the total sinking).

The different response of the subpolar gyre to changes in thermohaline and wind forcing is demonstrated also in Fig. 10, showing maps of the vertically integrated mass transport streamfunction for several model cases discussed above. The gross transport pattern is similar for the basic 1/3° and 1° cases (Figs. 10a and 10b, respectively), except that with the higher resolution there are stronger regional recirculation cells in the Labrador and Irminger Sea, locally enhancing the boundary current transports. While even a complete shutdown of the wind stress (Fig. 10c) leads only to moderate changes in the gyre pattern compared to the reference case, the northern boundary condition does play a much stronger role: the gyre shrinks considerably in the case with no relaxation to prescribed hydrographic data (Fig. 10d), whereas the restoring to actual section data, which includes the cold DSOW core (Fig. 10e), gives rise to significantly enhanced gyre transports. Compared to this effect of thermohaline forcing at the northern boundary, the effect of the surface fluxes appears negligible; that is, there are no significant changes in the gyre pattern when the heat and freshwater fluxes are turned off over the subpolar North Atlantic (K1-NF).

c. *Meridional overturning and heat transport*

The effect of different restoring data in the northern buffer zone on the vertical structure of the overturning cell has been examined by Döscher et al. (1994). In the 1° model with actual section data capturing the signature of DSOW (case K1-C2), the AABW overturning cell is almost eliminated, while the southward transport of NADW between 3000 and 5000 m is greatly enhanced compared to a case using climatological restoring data (Fig. 11a). The effect is somewhat less drastic in the 1/3° model, with southward flow in the actual section case (K13-6) extending down to 4400 m, compared to 3900 m in the basic case. The role of the northern boundary condition is further demonstrated in the 1° case without any restoring (Fig. 11b). The southward transport becomes even more concentrated in the upper deep-water range: the level of zero meridional flow rises to 3100 m, from 4200 m in the standard 1° case. A similar, but weaker tendency occurs when going from 1° to 1/3° resolution (and to a narrower buffer zone) (Fig. 11c): the zero level rises to 3900 m, reflecting the less effective buffer zone in the high-resolution cases.

The restoring to climatological data in the southern buffer zone also has an effect both on the NADW and the AABW overturning cells. Without that restoring, there is no forcing of the lower cell resulting in very weak meridional transports in the deeper layers (Fig. 11d). In addition, the water mass transformations enforced in the southern buffer zone have a significant influence on the NADW transport throughout the model domain. Without restoring, the flow of deep water into the southern buffer zone nearly ceases, which effectively brakes the meridional overturning over the whole North Atlantic: the deep-water production in the north is reduced to 8.8 Sv (Table 2), and the NADW transport across 25°N falls to less than 4 Sv.

The strength of the NADW overturning cell in the subtropical and tropical North Atlantic is strongly affected by the upwelling of deep water in the western boundary layer of the midlatitudes (Fig. 1a). Böning et al. (1995) noted that for model cases with the same grid resolution and mixing parameterization, the upwelling correlates with the upper-layer, northward transport of the western boundary current. The net change in the overturning rate of the NADW cell between 47° and 25°N is examined in Table 4, for a num-

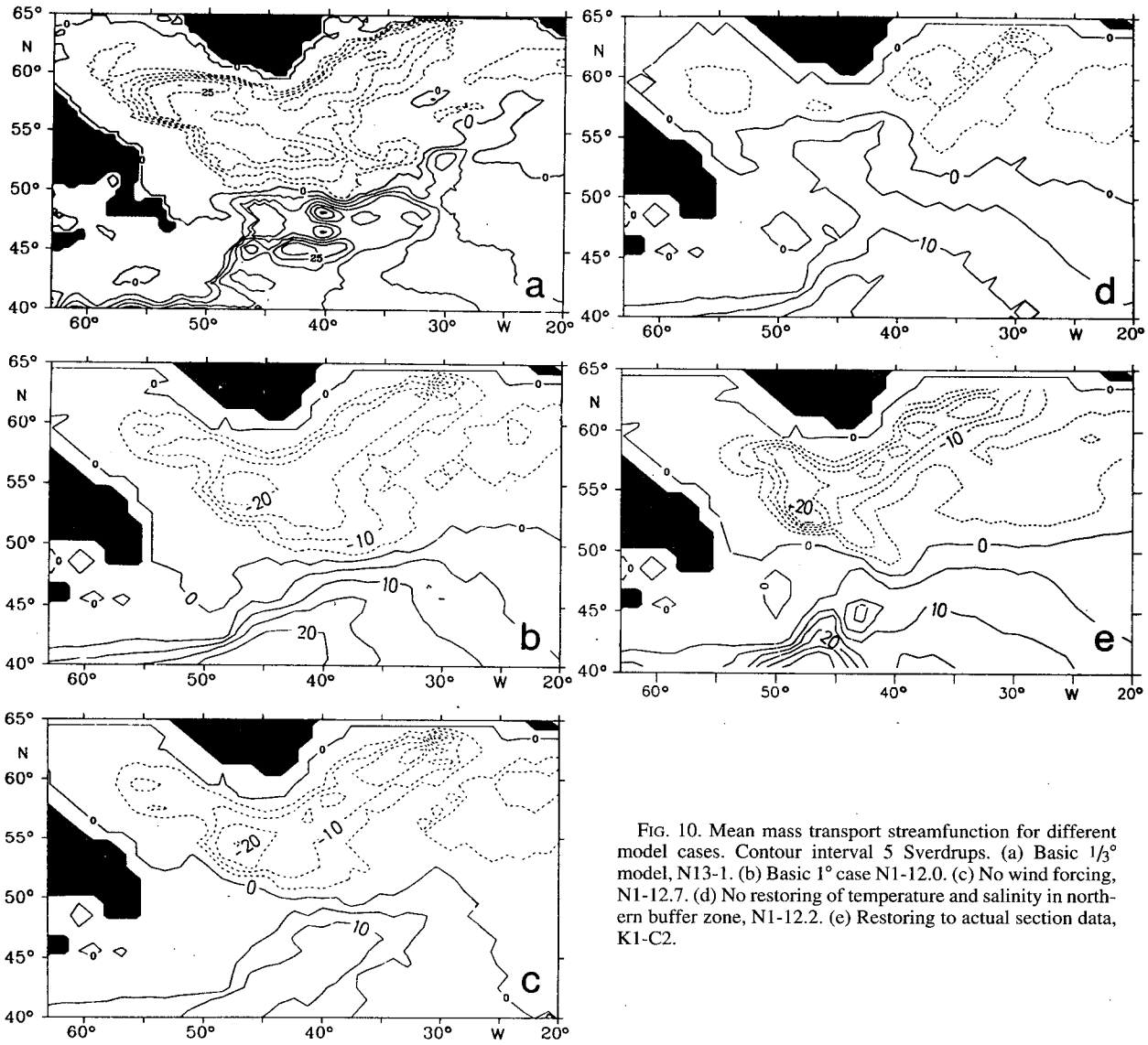

FIG. 10. Mean mass transport streamfunction for different model cases. Contour interval 5 Sverdrups. (a) Basic 1/3° model, N13-1. (b) Basic 1° case N1-12.0. (c) No wind forcing, N1-12.7. (d) No restoring of temperature and salinity in northern buffer zone, N1-12.2. (e) Restoring to actual section data, K1-C2.

ber of model cases that differ in thermohaline forcing, wind forcing, and mixing parameterization. Especially illuminating are the effects of the artificial changes in the wind forcing in the 1° version. If the wind stress and thus the subtropical gyre transport is increased (case N1-12.5), the upwelling is enhanced (7.0 Sv compared to 6.1 Sv in the reference case), weakening the overturning rate at 25°N even further (8.5 Sv vs 10.5 Sv). An opposite effect can be seen if the wind forcing is turned off (N1-12.7): the weaker Gulf Stream (14 Sv at 25°N compared to 27.8 Sv in the reference case) is associated with a weaker upwelling (4.4 Sv), bringing the overturning rate at 25°N up to 15.8 Sv. The midlatitude upwelling is somewhat weaker in the high-resolution model (5.1 Sv in the basic case). Differences in gyre transport among the 1/3° cases using different wind stress climatologies are not strong enough to cause significant effects on the net overturning rate in the subtropical Atlantic.

Table 4 indicates a much smaller midlatitude upwelling rate for several cases. As discussed in Böning et al. (1995), there is a beneficial effect of a smaller ratio of horizontal diffusivity to horizontal viscosity in model cases using a horizontal/vertical mixing scheme (cases N1-25.0 and K13-7). No net loss of deep water at all is found in model case N1-26.0 using the new parameterization of the effect of mesoscale eddies developed by Gent and McWilliams (1990), which includes mixing along isopycnal surfaces, not in the horizontal. Danabasoglu et al. (1994) show similar effects for a coarsely resolved equilibrium global ocean solution. There is also almost no difference between the

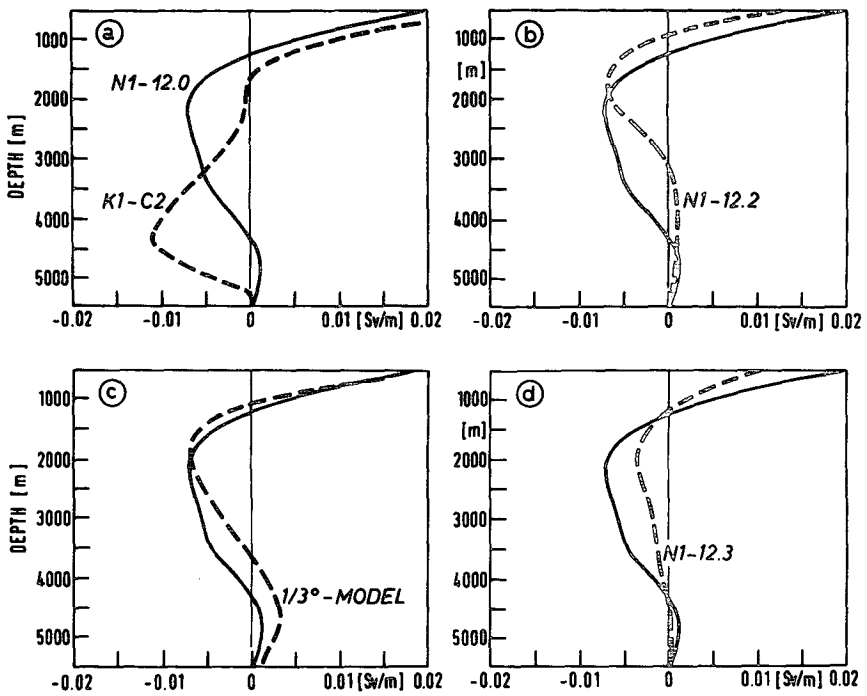

FIG. 11. Vertical profiles of meridional mass transport per unit depth at 36°N for different model cases. The profile for the 1° case with restoring to climatological data in the northern and southern buffer zones (N1-12.0) serves as a reference (thin continuous line). (a) Restoring to actual section data (K1-C2), and (b) no restoring (N1-12.2) in the northern buffer zone. (c) 1/3° model with climatological restoring. (d) No restoring in the southern buffer zone (N1-12.3).

overturning rates at 25° and 47°N in the 1° model with restoring to actual section data in the northern buffer zone (K1-C2).

A small net vertical transport in the zonally integrated budgets does not imply a small upwelling in the western boundary layer. A significantly smaller regional upwelling along the Gulf Stream is only found in the cases with a reduced ratio of diffusivity to viscosity. A net upwelling of 3.4 Sv occurs in a strip approximately 10° wide along the western boundary in N1-25.0 compared to 6.1 Sv in the basic case N1-12.0. In the other two cases mentioned above, there is a substantial regional upwelling across 1000 m: 4.9 Sv in N1-26.0 and 6.7 Sv in K1-C2. The sources of the upwelling water are very different. While in the basic cases the vertical transport draws upon the southward flowing deep water and thus affects the meridional overturning cell, the upwelling in the isopycnal mixing case (N1-26.0) is fed by water that sinks to the east of the Gulf Stream. In the case with actual section data in the northern buffer zone (K1-C2), the center of the meridional overturning cell is shifted to a much deeper level (Fig. 11a) so that upwelling at the 1000-m level does not affect the deep water but rather the northward flowing intermediate water.

Finally, let us examine the host of CME cases with respect to the effects of resolution, different deep-water production rates, and different midlatitude upwelling patterns on the meridional transport of heat. As shown in Table 4, the heat transports at 25°N vary over a wide range from 0.45 to 1.0 PW. Figure 12 shows that the heat transport at this latitude approximately covaries with the local strength of the NADW cell: it increases by about 0.1 PW for a 2 Sv gain in overturning. (Not included here is case K1-C2; its vertical mass transport profile strongly differs from the other cases.) The dependence suggests, on average for the model cases displayed, a net effect of the wind-driven circulation (horizontal gyre plus Ekman transport) of 0.2–0.3 PW at this latitude.

As suggested by the previous discussion and indicated in Table 4, one may identify two very different mechanisms for obtaining a larger, more realistic overturning rate and heat transport at 25°N than in the basic (high or coarse resolution) model cases. The obvious one is an increased overall overturning rate in the North Atlantic by a stronger thermohaline forcing and deep-water production in subpolar areas. An increase by 0.2–0.3 PW is obtained, for example, by restoring to hydrographic data based on an actual section near 65°N, instead to smoothed climatological data as in the basic cases. Of similar importance for the heat transport in the lower latitudes is how much of the deep water exported from the subpolar North Atlantic is lost due

TABLE 4. Maxima of the NADW overturning cell at 47° and 25°N (in Sv) and northward heat transport at 25°N (in PW) for model cases differing in horizontal resolution, thermohaline forcing, and mixing parameterization.

Model case		Mass transport 47°N	Mass transport 25°N	Heat transport 25°N
(I) Effect of thermohaline forcing				
(a) 1° version				
No northern restoring	(N1-12.2)	11.8	5.4	0.45
Climatological restoring	(N1-12.0)	16.6	10.5	0.70
Actual section	(K1-C2)	20.0	20.2	1.0
(b) 1/3° version				
Climat. restoring	(K13-2)	11.9	6.3	0.61
Actual section	(K13-6)	15.0	11.9	0.82
(II) Effect of wind forcing				
Basic case	(N1-12.0)	16.6	10.5	0.70
No wind	(N1-12.7)	20.2	15.8	0.77
Stronger wind	(N1-12.5)	15.5	8.5	0.66
(III) Effect of mixing parameterization				
(a) 1° version				
Reference case	(N1-12.0)	16.6	10.5	0.70
Reduced A_h/A_m	(N1-25.0)	15.3	11.9	0.78
$G - M$ mixing	(N1-26.0)	16.5	17.4	0.98
(b) 1/3° version				
Reference case	(K13-6)	15.0	11.9	0.82
Reduced A_h/A_m	(K13-7)	15.0	13.2	0.94

to the spurious upwelling in the midlatitudes. In order to assess the effect of these different mechanisms more thoroughly it is necessary to consider not only the northward heat transports at a single latitude but to examine their latitudinal distributions. Figure 13a shows the heat transport from the basic model case in comparison to two observational studies: the results of Isemer et al. (1989, hereafter IHW), based on the surface heat fluxes and an inverse method using a northward oceanic heat transport of 1 PW at 25°N as a constraint to adjust the bulk coefficients for the air–sea transfers within their meteorological range of uncertainty, and the results of Trenberth and Solomon (1994) from the top-of-the-atmosphere radiation balance and the atmospheric energy divergence. Both show much larger northward heat transports than the basic model in the Tropics and subtropics but rather small deviations in higher latitudes north of 35°–40°N.

The influence of thermohaline forcing at the northern boundary is displayed in Figs. 13b–d. The different magnitudes of the northward heat transport in the non-eddy- and eddy-resolving cases, as illustrated in Fig. 13b, have to be considered primarily as a consequence of differences in the efficiency of the buffer zones and in the magnitude of the midlatitude upwelling and thus do not allow conclusions about the net effect of the eddy fluxes. [The partition of H in mean and eddy fluxes for the 1/3° and 1/6° models is discussed in Bryan and Holland (1989) and Beckmann et al. (1994a).] The heat transport of the 1° basic case, with a net sinking of more than 16.6 Sv, already tends to be somewhat larger than observed in the subpolar North Atlantic. A further increase of the deep-water production as in K1-C2 leads to an even stronger excess in these latitudes (Fig. 13c). A similar tendency is obtained for the high-resolution counterpart K13-6 (Fig. 13d), while a large deficit remains in the subtropics and Tropics. Figures 13e, f show significant increases in the low-latitude heat transports for the cases with less amounts of mid-latitude upwelling. Neither in the high-resolution case with the smaller A_h/A_m ratio (K13-7) nor in the non-eddy-resolving case with the isopycnic mixing scheme (N1-26.0) is there a significant change in the high latitudes.

5. Discussion and conclusions

A question of particular interest is which areas and processes in the subpolar North Atlantic contribute to the renewal of deep water and which factors control the sinking rate and hence the intensity of the meridional overturning circulation. While the principal source regions for the deep water masses in the North Atlantic are reasonable well known from hydrographic and tracer observations, there are only few quantitative measurements of the mass transport distribution in the subpolar North Atlantic, for example, Clarke (1984) and Dickson et al. (1991). Hence, very little is known about the dynamics of the system; that is, where does the sinking actually take place and how does the mass transport respond to changes in the atmospheric forcing fields? Perhaps the most striking model result in this regard is the small dynamical effect of deep winter mixing in the Labrador Sea on the large-scale circulation.

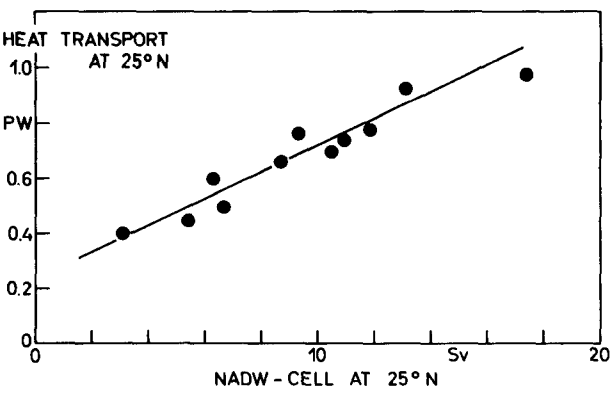

FIG. 12. Northward heat transport at 25°N against meridional overturning at 25°N, for model cases that differ in thermohaline forcing at the northern boundary, wind forcing, mixing parameterization and horizontal resolution (see Table 4).

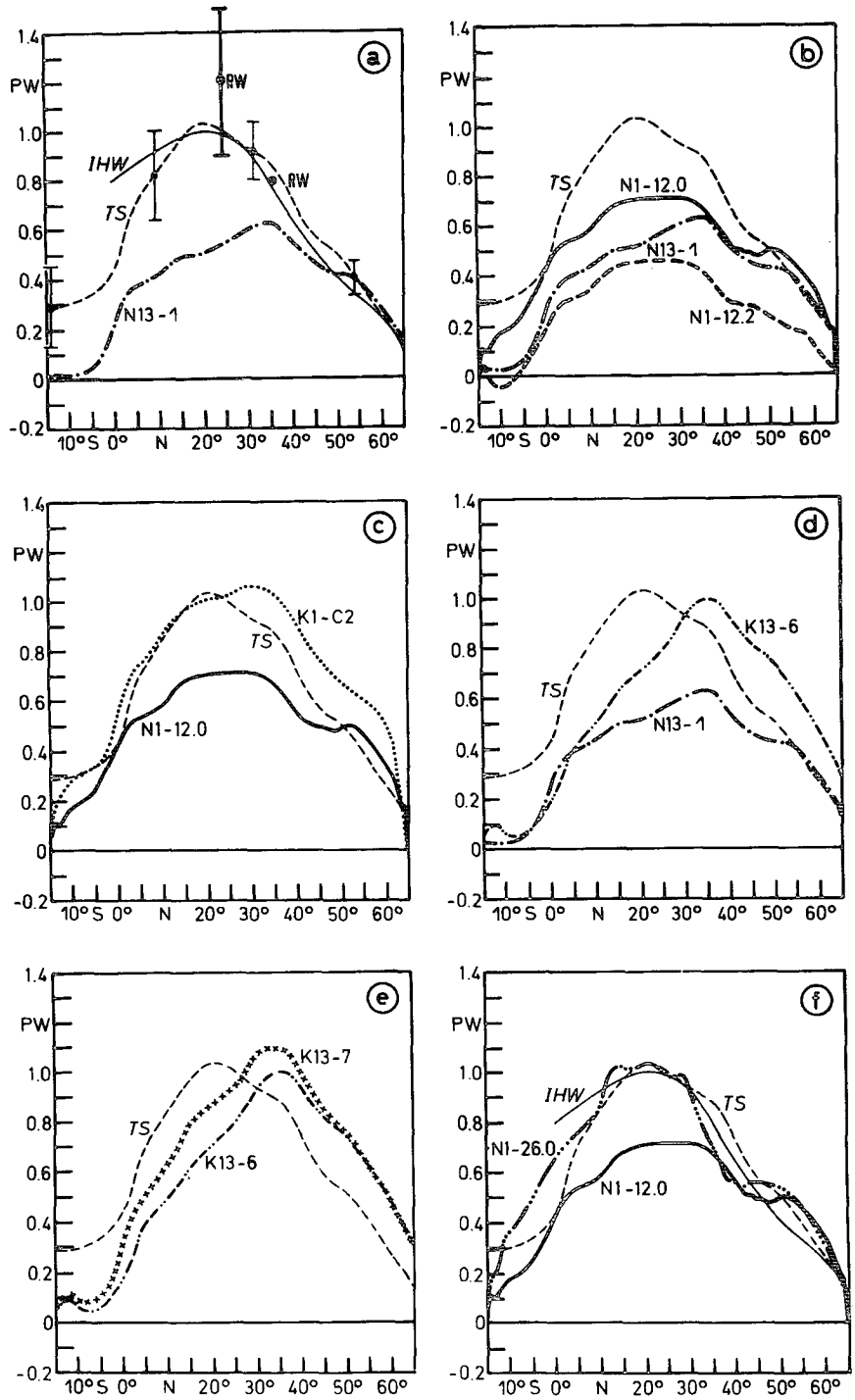

FIG. 13. Northward heat transport as function of latitude for different model cases, in comparison to the observational estimates of Isemer et al. (1989; denoted IHW) and Trenberth and Solomon (1994; denoted TS). (a) Basic 1/3° model (N13-1), (b) comparison with basic 1° model (N1-12.0) and case without restoring in northern buffer zone (N1-12.2), (c) effect of restoring to actual section data for the 1° case (K1-C2) and (d) for the 1/3° case (K13-6), (e) effect of reduced ratio of horizontal diffusivity to viscosity in the 1/3° model (K13-7), (f) effect of the isopycnal mixing scheme developed by Gent and McWilliams (1989) (N1-26.0).

All versions of the CME seem to be able to reproduce the major features of the water mass transformation due to surface cooling in this area: vertical mixing during winter generates deep (2000 m) columns of homogenized water in the center and near the northwestern perimeter of the Labrador Sea. The hydrographic properties of the main patch in the center of the gyre are similar to the observations of Clarke and Gascard (1983) after a winter with deep convection, with θ somewhat less than 3°C and S about 34.85 psu. However, in no model case is this an area with a sizable net sinking. Vertical transports across 1000 m are only 1 Sv or less over the whole Labrador Sea, much smaller than the equivalent annual production rate (about 5 Sv) one would get if all the homogenized water would exit the area.

A plausible interpretation of this result is that the deep mixing occurs in rather stagnant areas. In particular, the main homogeneous pool in the center of the gyre is not in close contact with the deep boundary current along the continental slope off Labrador so that there is no effective drainage of this water. Recently, Send and Marshall (1995) have investigated the large-scale, integral effect of the ensemble of convective "plumes" comprising an open-ocean chimney, using scaling ideas derived from physical arguments and tested against finescale nonhydrostatic model results. Their principal conclusion is that convection basically acts as a mixing agent that effectively homogenizes a vertical column of water, without generating significant mean vertical motion. The outflow of dense water should be controlled by horizontal exchange processes involving baroclinic instability and eddies.

The small sinking rate in the area with deepest winter mixing, a robust result of all CME cases, has important implications for the dynamics of the thermohaline circulation. Changes in the surface buoyancy fluxes over the subpolar North Atlantic, even if they lead to a complete shutdown of deep convective mixing in the Labrador Sea, have very little effect on the net sinking and meridional overturning rate on the decadal timescales of the model integrations. (Additional model analyses, not presented here, show that changes in the strength of winter mixing in the Labrador Sea affect the hydrographic conditions of the upper NADW and the uptake and distribution of anthropogenic tracers.) The CME behavior appears to be in striking contrast to recent results from climate models related to the question of interdecadal variability. Delworth et al. (1993) present a coupled ocean–atmosphere model that shows interdecadal oscillations of the thermohaline circulation driven by density variations in the western subpolar North Atlantic. Weisse et al. (1994) present results of a stochastically forced ocean model that shows oscillations on decadal timescales associated with the generation of salinity anomalies in the (idealized) Labrador Sea. In both cases, there is a dynamical relation between temperature and salinity anomalies over the western portion of the subpolar gyre and the intensity of the meridional overturning circulation. The distribution of the convection and sinking regions is shown in neither case, but we may assume that an effective regional separation as obtained in the CME is not likely to occur in models with 4°–5° resolution. The different dynamical response to anomalies in the surface buoyancy fluxes in the CME raises the question of how robust, and hence how realistic, the results of coarse-resolution models are regarding the mechanisms of the thermohaline circulation.

Both the renewal of deep water and the distribution of the horizontal mass transport field in the subpolar North Atlantic are effectively controlled by the conditions applied near the northern model boundary at 65°N. The version of the CME discussed here attempts to mimic the effect of the outflow of dense waters from the Nordic Seas by restoring the predicted temperatures and salinities near the northern boundary (east of Greenland) to observed values. The subpolar gyre is essentially governed by the generation of DSOW in the buffer zone between Greenland and Iceland. Without the buffer zone, the subpolar gyre is virtually absent. With the buffer zone, the horizontal mass transport strongly depends on the restoring data; it exceeds 30 Sv if actual section data are used, comparing favorably with the observational estimate of 34 Sv given by Clarke (1984). In contrast, changes in the wind forcing have only a small effect on the subpolar gyre transport. (Note, however, that an implicit effect of the wind field is also present in the relaxation conditions used for the buoyancy forcing.) This result appears consistent with the diagnostic model calculations of Greatbatch et al. (1991) who found that the contribution of (explicit) wind forcing to the subpolar gyre transport is very small (about 2 Sv) compared to the contribution by the joint effect of baroclinicity and relief. The vorticity balance of the CME mass transport fields are examined by Bryan et al. (1995a), showing strong deviations from linear Sverdrup dynamics and the importance of higher-order dynamics across the entire extent of the subpolar gyre.

A major problem of the buffer zone approach concerns the circulation in the eastern part of the subpolar North Atlantic. Probably because east of Iceland the model boundary and adjacent buffer zone (or, in the 1° version, a major fraction of it) lie north of the ridge region, there is only a small exchange of flow with the Atlantic proper. This affects the course of the NAC which, depending on the particular choice of restoring data, develops a more or less strong tendency to flow north toward the Denmark Straits, leaving the eastern basin far too quiet energetically. Obviously, the regional circulation patterns in the northeastern Atlantic can only be improved if a significant fraction of the NAC is allowed to flow into the Iceland Basin and to exit between Iceland and Scotland, for example, by us-

ing open boundary conditions or an expanded domain that permit an exchange of mass with the Nordic Seas.

The meridional overturning cell associated with the renewal and southward transport of NADW is of prime importance for the poleward transport of heat in the North Atlantic. The heat transport at 25° covaries with the local intensity of the overturning: it roughly increases by 0.1 PW for a 2 Sv gain in meridional overturning at that latitude. Since the net contribution of the wind-driven circulation at 25°N is 0.2–0.3 PW (the four different wind stress climatologies used for the model account for only small changes in the heat transport), we need an overturning intensity of about 15 Sv at this latitude to obtain a northward heat transport of 1 PW.

Two main factors affecting the spatial structure and intensity of the NADW overturning cell have been elucidated by the host of CME experiments: the conditions in the DSOW outflow region (Döscher et al. 1994), and the spurious upwelling of deep water in the Gulf Stream regime (Böning et al. 1995). In the $1/3°$ model using actual section data in the northern buffer zone (K13-6), the net formation of NADW in the subpolar North Atlantic is 15 Sv, compared to about 12 Sv in the cases with climatological restoring. Of prime importance for the upwelling pattern is the parameterization of horizontal mixing, which in turn depends on the grid resolution of the model. In order to eliminate horizontal diffusion as a leading order term in the heat budget of the Gulf Stream Front in eddy-resolving models using biharmonic horizontal mixing schemes, a possibility is to widen the front by increasing the viscosity as in case K13-7. The significantly weaker upwelling in this case appears consistent with results from a recent version of the $1/2°$ global ocean model of Semtner and Chervin (1992) (in which the restoring to climatology in the deep ocean used in the original version was skipped). With the coefficient for biharmonic friction three times larger than that for diffusion, that model exhibits only a small loss of deep water in the midlatitude North Atlantic (R. Chervin 1994, personal communication). For non-eddy-resolving models, the best alternative seems to be a parameterization of eddy mixing in the spirit of Gent and McWilliams (1990) that does include along-isopycnal, but no horizontal, diffusion of tracers. Details of the vertical circulation and its dynamics in the western boundary region are complicated, however, and need to be investigated further.

The CME experiments indicate a number of subtle effects of model resolution with far-reaching implications for the dynamics of the meridional overturning circulation and heat transport in the North Atlantic. In particular, the apparently minor role of mesoscale eddies in the heat balance of the time mean circulation (Bryan 1986; Böning and Budich 1992; Drijfhout 1994; Beckmann et al. 1994a) cannot readily be taken to justify the use of coarse-resolution models for the simulation of large-scale ocean transport. A realistic representation of the oceanic frontal features, energetic flow structures, and small-scale processes involved in the formation of NADW, appears to be a prerequisite to an understanding of the dynamics of the thermohaline circulation and a simulation of its role in climate variations.

Acknowledgments. We would like to thank Julianna Chow and Peter Herrmann for their assistance in the integration and analysis of the CME model. CB and RD were supported by the Deutsche Forschungsgemeinschaft. FB and WH were supported by the National Science Foundation through its sponsorship of the National Center for Atmospheric Research.

REFERENCES

Beckmann, A., C. W. Böning, C. Köberle, and J. Willebrand, 1994a: Effects of increased horizontal resolution in a simulation of the North Atlantic Ocean. *J. Phys. Oceanogr.*, **24,** 326–344.

——, ——, B. Brügge, and D. Stammer, 1994b: On the generation and role of eddy variability in the central North Atlantic Ocean. *J. Geophys. Res.*, **99,** 20 381–20 391.

Böning, C. W., and R. G. Budich, 1992: Eddy dynamics in a primitive equation model: Sensitivity to horizontal resolution and friction. *J. Phys. Oceanogr.*, **22,** 361–381.

——, W. R. Holland, F. O. Bryan, G. Danabasoglu, and J. C. McWilliams, 1995: An overlooked problem in model simulations of the thermohaline circulation and heat transport in the Atlantic Ocean. *J. Climate,* **8,** 515–523.

Broecker, W. G., 1991: The great ocean conveyor. *Oceanography,* **4,** 79–89.

Bryan, F. O., 1987: Parameter sensitivity of primitive equation ocean general circulation models. *J. Phys. Oceanogr.*, **17,** 970–985.

——, and W. R. Holland, 1989: A high resolution simulation of the wind- and thermohaline-driven circulation in the North Atlantic Ocean. *Parameterization of Small-Scale Processes,* Proc. 'aha huliko'a, Hawaiian Winter Workshop, University of Hawaii, 99–115.

——, C. W. Böning, and W. R. Holland, 1995a: On the midlatitude circulation in a high-resolution model of the North Atlantic. *J. Phys. Oceanogr.*, **25,** 289–305.

——, I. Wainer, and W. R. Holland, 1995b: Sensitivity of the tropical Atlantic circulation to specification of wind stress climatology. *J. Geophys. Res.*, **100,** 24 729–24 744.

Bryan, K., 1969: A numerical method for the study of the circulation of the World Ocean. *J. Comput. Phys.*, **4,** 347–376.

——, 1986: Poleward buoyancy transport in the ocean and mesoscale eddies. *J. Phys. Oceanogr.*, **16,** 927–933.

——, and J. L. Sarmiento, 1985: Modeling ocean circulation. *Advances in Geophysics,* Vol. 28A, Academic Press, 433–459.

Clarke, A., 1984: Transport through the Cape Farewell–Flemish cap section. *Rapp. P.-V. Reun.-Cons. Int. Explor. Met.,* **185,** 120–130.

——, and J.-C. Gascard, 1983: The formation of Labrador Sea Water. Part I: Large scale processes. *J. Phys. Oceanogr.*, **13,** 1764–1778.

Cox, M. D., 1984: A primitive equation three-dimensional model of the ocean. GFDL Ocean Group Tech. Rep. No. 1, Geophysical Fluid Dynamics Laboratory/NOAA, Princeton, NJ, 56 pp.

——, 1987: Isopycnal diffusion in a z-coordinate model. *Ocean Modelling* (unpublished manuscript), **74,** 1–5.

Danabasoglu, G., J. C. McWilliams, and P. R. Gent, 1994: The role of mesoscale tracer transports in the global ocean circulation. *Science,* **264,** 1123–1126.

Delworth, T., S. Manabe, and R. J. Stouffer, 1993: Interdecadal variations of the thermohaline circulation in a coupled ocean–atmosphere model. *J. Climate,* **6,** 1993–2011.

Dickson, R. R., E. M. Gmitrowicz, and A. J. Watson, 1991: Deep-water renewal in the northern North Atlantic. *Nature,* **344,** 848–850.

Döscher, R., C. W. Böning, and P. Herrmann, 1994: Response of meridional overturning and heat transport in the North Atlantic to changes in thermohaline forcing in northern latitudes: A model study. *J. Phys. Oceanogr.,* **24,** 2306–2320.

Drijfhout, S. S., 1994: On the heat transport by mesoscale eddies in an ocean circulation model. *J. Phys. Oceanogr.,* **24,** 353–369.

England, M. H., 1993: Representing the global-scale water masses in ocean general circulation models. *J. Phys. Oceanogr.,* **23,** 1523–1552.

Fine, R. A., and R. L. Molinari, 1988: A continuous deep western boundary current between Abaco (26.5 N) and Barbados (13 N). *Deep-Sea Res.,* **35,** 1441–1450.

Gent, P. R., and J. C. McWilliams, 1990: Isopycnal mixing in ocean circulation models. *J. Phys. Oceanogr.,* **20,** 150–155.

Gerdes, R., 1993: A primitive equation ocean circulation model using a general vertical coordinate transformation. Part 2: Application to an overflow problem. *J. Geophys. Res.,* **98,** 14 703–14 726.

——, and C. Köberle, 1995: On the influence of DSOW in a numerical model of the North Atlantic general circulation. *J. Phys. Oceanogr.,* **25,** 2624–2642.

Greatbatch, R. J., A. F. Fanning, A. D. Goulding, and S. Levitus, 1991: A diagnosis of interpentadal circulation changes in the North Atlantic. *J. Geophys. Res.,* **96**(C12), 22 009–22 023.

Hall, M. M., and H. L. Bryden, 1982: Direct estimates of ocean heat transport. *Deep-Sea Res.,* **29,** 339–359.

Han, Y.-J., 1984: A numerical World Ocean circulation model. Part II: A baroclinic experiment. *Dyn. Atmos. Oceans,* **8,** 141–172.

Haney, R. L., 1971: Surface thermal boundary condition for ocean circulation models. *J. Phys. Oceanogr.,* **1,** 241–248.

Hellermann, S., and M. Rosenstein, 1983: Normal monthly wind stress over the World Ocean with error estimates. *J. Phys. Oceanogr.,* **13,** 1093–1104.

Holland, W. R., and F. O. Bryan, 1994: Sensitivity studies on the role of the ocean in climate change. *Ocean Processes in Climate Dynamics: Global and Mediterranean Examples.* P. Malanotte-Rizzoli and A. R. Robinson, Eds., NATO ASI Proc., Kluwer, 111–134.

Isemer, H.-J., and L. Hasse, 1987: *The Bunker Climate Atlas of the North Atlantic Ocean.* Vol. 2. *Air–Sea Interactions.* Springer Verlag, 256 pp.

——, ——, and J. Willebrand, 1989: Fine adjustment of large scale air–sea energy flux parameterizations by direct estimates of ocean heat transport. *J. Climate,* **2,** 1173–1184.

Kawase, M., 1987: Establishment of deep ocean circulation driven by deep-water production. *J. Phys. Oceanogr.,* **17,** 2294–2317.

Krauss, W., 1986: The North Atlantic Current. *J. Geophys. Res.,* **91,** 5061–5074.

——, and R. H. Käse, 1984: Mean circulation and eddy kinetic energy in the eastern North Atlantic. *J. Geophys. Res.,* **89,** 3407–3415.

Lazier, J. R. N., 1988: Temperature and salinity changes in the deep Labrador Sea, 1962–1986. *Deep-Sea Res.,* **35,** 1247–1253.

Levitus, S., 1982: *Climatological Atlas of the World Ocean.* NOAA Prof. Paper No. 13, U.S. Govt. Printing Office, Washington, D.C., 173 pp.

Maier-Reimer, E., U. Mikolajewicz, and K. Hasselmann, 1993: Mean circulation of the Hamburg LSG OGCM and its sensitivity to the thermohaline surface forcing. *J. Phys. Oceanogr.,* **23,** 731–757.

McCartney, M. S., 1992: Recirculating components to the deep boundary current of the northern North Atlantic. *Progress in Oceanography,* Vol. 29, Pergamon, 283–383.

——, and L. D. Talley, 1982: The subpolar mode water of the North Atlantic Ocean. *J. Phys. Oceanogr.,* **12,** 1169–1188.

——, and R. A. Curry, 1993: Trans-equatorial flow of Antarctic Bottom Water in the western Atlantic Ocean: Abyssal geostrophy at the equator. *J. Phys. Oceanogr.,* **23,** 1264–1276.

——, S. L. Bennett, and M. E. Woodgate-Jones, 1991: Eastward flow through the Mid-Atlantic Ridge at 11 N and its influence on the abyss of the eastern basin. *J. Phys. Oceanogr.,* **21,** 1089–1129.

Price, J. F., and M. O'Neil Baringer, 1994: Outflow and deepwater production by marginal seas. *Progress in Oceanography,* Vol. 33, Pergamon, 161–200.

Redi, M. H., 1982: Oceanic isopycnal mixing by coordinate rotation. *J. Phys. Oceanogr.,* **12,** 1154–1158.

Rintoul, S. R., 1991: South Atlantic interbasin exchange. *J. Geophys. Res.,* **96,** 2675–2692.

Roemmich, D., and C. Wunsch, 1985: Two transatlantic sections: Meridional circulation and heat flux in the subtropical North Atlantic Ocean. *Deep-Sea Res.,* **32,** 619–664.

Sarmiento, J. L., 1986: On the North and Tropical Atlantic heat balance. *J. Geophys. Res.,* **91,** 11 677–11 689.

Saunders, P. M., 1982: Circulation in the eastern North Atlantic. *J. Mar. Res.,* **40,** 641–657.

Schmitz, W. J., Jr., and W. S. Richardson, 1991: On the sources of the Florida Current. *Deep-Sea Res.,* **38,** 379–409.

——, and M. S. McCartney, 1993: On the North Atlantic circulation. *Rev. Geophys.,* **31,** 29–49.

Semtner, A. J., and R. M. Chervin, 1992: Ocean general circulation from a global eddy-resolving model. *J. Geophys. Res.,* **97,** 5493–5550.

Send, U., and J. Marshall, 1995: Integral effects of deep convection. *J. Phys. Oceanogr.,* **25,** 855–872.

Smethie, W. M., Jr., and J. H. Swift, 1989: The Tritium: Krypton-85 age of Denmark Strait overflow water and Gibbs Fracture Zone water just south of Denmark Strait. *J. Geophys. Res.,* **94,** 8265–8275.

Spall, M. A., 1990: Circulation in the Canary Basin: A model/data analysis. *J. Geophys. Res.,* **95,** 9611–9628.

Trenberth, K. E., and A. Solomon, 1994: The global heat balance: Heat transports in the atmosphere and ocean. *Climate Dyn.,* **10,** 107–134.

Weaver, A. J., J. Marotzke, P. F. Cummins, and E. S. Sarachik, 1993: Stability and variability of the thermohaline circulation. *J. Phys. Oceanogr.,* **23,** 39–60.

Weisse, R., U. Mikolajewicz, and E. Maier-Reimer, 1994: Decadal variability of the North Atlantic in an ocean general circulation model. *J. Geophys. Res.,* **99,** 12 411–12 421.